Knickpoint formation, rapid propagation, and landscape response following coastal cliff retreat at the last interglacial sea-level highstand: Kaua‘i, Hawai‘i

Benjamin H. Mackey†, Joel S. Scheingross, Michael P. Lamb, and Kenneth A. Farley
Division of Geological and Planetary Sciences, California Institute of Technology, Pasadena, California 91125, USA

ABSTRACT

Upstream knickpoint propagation is an important mechanism for channel incision, and it communicates changes in climate, sea level, and tectonics throughout a landscape. Few studies have directly measured the long-term rate of knickpoint retreat, however, and the mechanisms for knickpoint initiation are debated. Here, we use cosmogenic ^{3}He exposure dating to document the retreat rate of a waterfall in Ka'ula'ula Valley, Kaua‘i, Hawai‘i, an often-used site for knickpoint-erosion modeling. Cosmogenic exposure ages of abandoned surfaces are oldest near the coast (120 ka) and systematically decrease with upstream distance toward the waterfall (<10 ka), suggesting that the waterfall migrated nearly 4 km over the past 120 k.y. at an average rate of 33 mm/yr. Upstream of the knickpoint, cosmogenic nuclide concentrations in the channel are approximately uniform and indicate steady-state vertical erosion at a rate of ~0.03 mm/yr. Field observations and topographic analysis suggest that waterfall retreat is dominated by block toppling, with sediment transport below the waterfall actively occurring by debris flows. Knickpoint initiation was previously attributed to a submarine landslide ca. 4 Ma; however, our dating results, bathymetric analysis, and landscape-evolution modeling support knickpoint generation by wave-induced sea-cliff erosion during the last interglacial sea-level highstand ca. 120–130 ka. We illustrate that knickpoint generation during sea-level highstands, as opposed to the typical case of sea-level fall, is an important relief-generating mechanism on stable or subsiding steep coasts, and likely drives transient pulses of significant sediment flux.

†Current address: Department of Geological Sciences, University of Canterbury, Private Bag 4800, Christchurch, New Zealand; ben.mackey@canterbury.ac.nz.

INTRODUCTION

Unlike landscapes undergoing continuous tectonic uplift, where erosion can balance uplift rates, resulting in steady-state topography (Whipple and Tucker, 1999; Willett et al., 2001), the life cycle of volcanic islands is dominated by transiently adjusting topography, which has the potential to better reveal the dominant geomorphic processes (e.g., Whipple, 2004; Bishop et al., 2005; Tucker, 2009; Ferrier et al., 2013a; Menking et al., 2013; Ramalho et al., 2013). In volcanic island chains such as Hawai‘i, the process of transient surface evolution is striking: Following the initial constructional phase of island growth, older islands subside and become progressively eroded as they move away from the active volcanic hotspot. One can readily observe differences in the morphology of volcanic islands of different ages along the hotspot chain, transitioning from broad convex volcanic shields (as seen on the Island of Hawai‘i) to the deeply incised landscape of Kaua‘i (Stearns, 1985). The template of a broad volcanic shield destined to undergo long-term subsidence and erosion renders volcanic islands a well-constrained setting to study the processes and rates of landscape evolution.

A prevailing viewpoint is that surface processes on volcanic islands are most active early in the island's life cycle: Shortly after the shield-building stage, when bedrock permeability begins to decline, forcing overland flow (e.g., Jefferson et al., 2010; Schopka and Derry, 2012), island centers sit high above sea level, and steep submarine slopes generate large flank failures (Moore et al., 1989). These landslides can lead to large-scale knickpoint retreat and fluvial incision (Seidl et al., 1994; Lamb et al., 2007). Despite the lack of tectonic uplift, surface processes on volcanic islands are surprisingly active and include cliff erosion, mass wasting, stream incision, and drainage capture. This is true even on older islands that have undergone substantial subsidence and submergence; for example, the 5-m.y.-old island of Kaua‘i, Hawai‘i, has modern erosion rates in line with those measured over thousands of years and inferred over millions of years (Gayer et al., 2008; Ferrier et al., 2013b). This finding suggests island evolution is richer than simple topographic decay and submergence, and it indicates the possibility of persistent high rates of erosion and local relief generation.

One possible mechanism for local relief generation on an actively subsiding landscape is stream response to back wearing of coastal cliffs by wave attack (Stearns, 1985). Indeed Stearns (1985) inferred that large waterfalls prevalent in canyons on the Hawai‘ian islands resulted from upstream-propagating knickpoints generated at wave-eroded coastal cliffs, and such a mechanism has been proposed for other coastal landscapes (Leyland and Darby, 2009; Ye et al., 2013). Other workers pointed to groundwater seepage erosion as a driver for knickpoint formation and retreat on Hawai‘ian islands (Hinds, 1925; Wentworth, 1928; Kochel and Piper, 1986). However, both sea-cliff erosion by waves and seepage erosion have fallen out of favor since the discovery of large deep-seated landslide deposits offshore of many Hawai‘ian volcanic islands (Moore et al., 1989, 1994; McMurtry et al., 2004). Seidl et al. (1994) and Lamb et al. (2007) inferred that sea cliffs and retreating knickpoints on Kaua‘i and the Island of Hawai‘i were generated following deep-seated flank collapse.

Beyond volcanic islands, the retreat of knickpoints and waterfalls (i.e., both slope-break and vertical step knickpoints; sensu Haviv et al., 2010; Kirby and Whipple, 2012) is recognized as a key mechanism by which perturbations in climate (Fuller et al., 2009), base level (Snyder et al., 2000; Bishop et al., 2005), and tectonics (Dorsey and Roering, 2006) are transmitted through a landscape (Crosby and Whipple, 2006; Berlin and Anderson, 2007). To calibrate and test numerical and mechanical models for knickpoint propagation, we need well-

GSA Bulletin; doi: 10.1130/B30930.1; 11 figures; 2 tables.

constrained field examples of knickpoint retreat rates and mechanisms. Despite the importance of waterfall migration in channel incision and landscape evolution, there are few direct measurements of rates on upstream propagation over 10^4–10^5 yr time scales (Loget and Van Den Driessche, 2009; Jansen et al., 2011; Whittaker and Boulton, 2012). Instead of direct measurements, most studies that have quantified rates of knickpoint retreat assume knickpoints were initiated by a major event of known age, such as isostatic rebound (Bishop et al., 2005), eustatic sea-level fall (Crosby and Whipple, 2006; Loget and Van Den Driessche, 2009), differential rates of channel incision (Berlin and Anderson, 2007), the initiation of faulting (Wobus et al., 2006), or large landslides (Seidl et al., 1994; Lamb et al., 2007).

One of the most popular testing grounds of knickpoint retreat consists of the valleys that drain to the Na Pali coast on Kaua‘i, Hawai‘i (Seidl et al., 1994, 1997; Stock and Montgomery, 1999; DeYoung, 2000; Chatanantavet and Parker, 2005; Ferrier et al., 2013a). This landscape is favored because the catchments are small with low-order drainages, lithology is uniform and well dated (Clague and Dalrymple, 1988), and topography prior to valley incision can be reconstructed due to relict primary volcanic surfaces preserved on ridgelines (Wentworth, 1927; Seidl et al., 1994; Stock and Montgomery, 1999; Ferrier et al., 2013a). Previous work has suggested that the knickpoints were initiated following a large-scale collapse of Kaua‘i’s northern flank shortly after volcano construction (Seidl et al., 1994, 1997; DeYoung, 2000), estimated to have occurred ~4 m.y. ago (e.g., McMurtry et al., 2004). This notwithstanding, the age and retreat rate for knickpoints on the Na Pali coast have not been measured directly, and thus the hypothesis of knickpoint generation by large-scale flank collapse has not been confirmed at this site. In an early application of cosmogenic nuclide dating, Seidl et al. (1997) attempted to measure the waterfall retreat rate in Ka’ula’ula Valley, Kaua‘i, but the results were largely inconclusive. Since the work of Seidl et al. (1997), improvement in cosmogenic nuclide exposure dating methods has proven the technique a valuable tool for measuring long-term rates of both channel incision and knickpoint retreat (e.g., Weissel and Seidl, 1998; Reusser et al., 2004; Righter et al., 2010; Valla et al., 2010; Abbuhl et al., 2011; Jakica et al., 2011; Jansen et al., 2011).

Herein, we revisit the evolution of Ka’ula’ula Valley through new cosmogenic dating, field observations, and topographic and bathymetric analysis. We first introduce the study location. Second, we present methods and results from ^{3}He exposure dating that indicate that the knickpoint initiated ca. 120 ka, i.e., much more recently than inferred from flank collapse (ca. 4 Ma), and has retreated at a near-constant rate of ~33 mm/yr. Third, we compare our measured waterfall retreat rate to models of knickpoint propagation, and we discuss field observations of erosion processes and sediment transport by debris flows. Fourth, we use topographic analysis to analyze hillslope evidence for knickpoint retreat. Fifth, we evaluate possible knickpoint retreat mechanisms and present landscape-evolution modeling that supports knickpoint initiation by wave-induced sea-cliff erosion during the last interglacial sea-level highstand (ca. 120–130 ka). Finally, we discuss erosion and transport mechanisms, and we place our results in the broader context of oceanic-island evolution.

KA’ULA’ULA VALLEY, KAUA‘I, HAWAI‘I

Kaua‘i is the second-oldest major subaerial island in the mantle-plume–produced Hawai‘ian volcanic chain, reaching 1593 m in elevation with an area of 1456 km^2 (Fig. 1). Thinly bedded tholeiitic shield-building lavas (5.1–4.0 Ma) comprise the original volcano structure and are exposed across much of the island (McDougall, 1979; Clague and Dalrymple, 1988). Following the shield-building phase, there was little volcanic activity for ~1 m.y. This hiatus was followed by caldera filling and rejuvenated volcanism of the Koloa Group (Maaloe et al., 1992), emplaced from 2.5 to 0.15 Ma (Garcia et al., 2010). Structurally, Kaua‘i is the most complex of the subaerial Hawai‘ian islands, with extensive faulting and flank collapse following the primary shield-building phase (Macdonald et al., 1960; Sherrod et al., 2007).

Ka’ula’ula Valley (Figs. 1 and 2) sits on the Na Pali coast, which is largely unaffected by the faulting and rejuvenated volcanism common to the central and eastern parts of the island (Sherrod et al., 2007), preserving the original shield volcano structure. This northwestern sector of Kaua‘i is composed of layered basalt that dips ~6° toward the coast (Macdonald et al., 1960); the Na Pali formation in this area has a mean age of 4.37 ± 0.11 Ma determined from K-Ar dating (McDougall, 1979). Along the Na Pali coast, the basalt beds are truncated by steep coastal cliffs up to 500 m high. The southern section of the cliffs is separated from active coastal processes by the Mana Plain (Fig. 2), and the abandoned sea cliffs have 30–40-m-tall talus piles near their base. Previous cosmogenic ^{3}He exposure dating of the abandoned sea cliffs just north of Ka’ula’ula Valley returned ages up to 30 ka (Mukhopadhyay et al., 2003), suggesting minimal cliff erosion during the Holocene, when the cliffs have been buffered from the sea by the northern Mana Plain.

Ka’ula’ula Valley is incised into the coastal cliffs and debouches on the Mana Plain, presently ~0.3 km from the coast (Fig. 2). The valley headwaters reach 1070 m elevation, and the channel is incised up to 250 m into the original shield volcano surface, as evident from relict surfaces preserved as broad interfluves between valleys (Fig. 2). Four kilometers from the valley entrance, the stream has a prominent 40-m-tall waterfall with a vertical headwall (Fig. 3C), which is our focus here, and there also exists a smaller (~10 m high) knickpoint 2.5 km further up the channel. The catchment’s upper reaches have likely been beheaded by enlargement of the Waimea Canyon (Seidl et al., 1994; Chatanantavet and Parker, 2005), reflected in the highly asymmetric ridge separating the Na Pali channels from the Waimea Canyon (Fig. 2). Although central Kaua‘i receives exceptionally high amounts of rainfall (up to 11 m/yr), the western coast is considerably drier. Annual rainfall at Ka’ula’ula Valley ranges from 0.6 m/yr on the Mana Plain to 1.4 m/yr in the upper catchment (PRISM Climate Group, Oregon State University, http://prism.oregonstate.edu). Abundant olivine phenocrysts in the basalt make the site well suited to cosmogenic dating using the isotope ^{3}He (Seidl et al., 1997; Gayer et al., 2008).

KNICKPOINT RETREAT RATES AND EROSION RATES

Here, we review previous work in Ka’ula’ula Valley and discuss field methods, sample preparation, and results from surface exposure age dating. All sample locations are projected to a longitudinal stream profile extracted from a high-resolution (~2 m spatial resolution) topographic data set collected from airborne light detecting and ranging (LiDAR). Herein, we use the term “accumulation age” to describe the generic accumulation of cosmogenic nuclides in a mineral sample. We calculated an accumulation age for stable isotopes using N/P, where N is measured concentration, and P is the nuclide production rate (e.g., Lal, 1991; Cerling and Craig, 1994). “Surface exposure ages” are accumulation ages interpreted to reflect the age of a geomorphic surface under the assumption of no subsequent surface erosion since the time of exposure. In a system undergoing erosion, on the other hand, accumulations ages are related to the average erosion rate, E (rather than the surface exposure age), as $E = \Lambda P/N$, where Λ is the e-folding length of cosmic rays at Earth’s surface (160 g/cm^2) or ~0.55 m in rock with

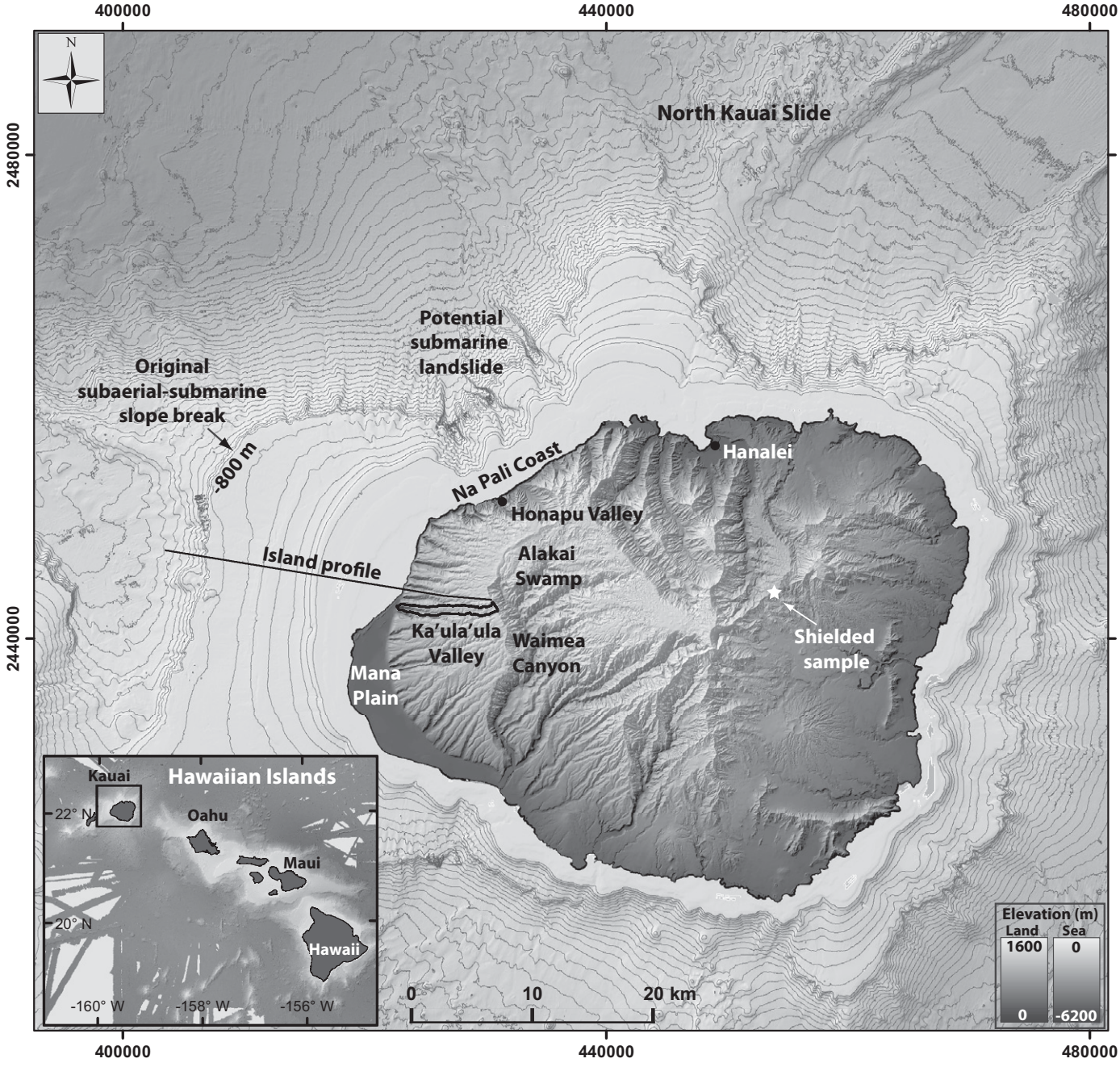

Figure 1. Topography and bathymetry of Kaua'i, Hawai'i. Ka'ula'ula Valley is outlined in black. The island profile used in Figure 9 is indicated as a solid black line. Bathymetric contour interval is 100 m. Bathymetry was obtained from the University of Hawai'i (http://www.soest.Hawai'i.edu/HMRG/multibeam/index.php), and topography is from the U.S. National Elevation Data Set. Inset shows bathymetry around the Hawaiian Islands with the region of the larger map outlined as a black square. Coordinate system is UTM Zone 4N.

density of 3 g/cm^3 (e.g., Niedermann, 2002). We choose to report the data as accumulation ages rather than nuclide concentrations (although these are also reported in Table 1) because they account for the dependence of nuclide production rate on elevation. We specify whether we interpret a given sample as an exposure age or an erosion rate.

Previous Work and Rationale

One of the earliest applications of cosmogenic isotopes to study channel incision and knickpoint retreat was undertaken by Seidl et al. (1997) in Ka'ula'ula Valley. Seidl et al. (1997) aimed to test the hypothesis that if valley evolution is dominated by waterfall retreat, there should be a predictable decrease in surface exposure ages of relict transport surfaces (e.g., terraces) moving upstream from the valley mouth to the waterfall (Fig. 4C). The basis for this argument is that down-valley sections removed from the active channel have been systematically eroded and left exposed by waterfall retreat for longer periods of time than those closer to the waterfall

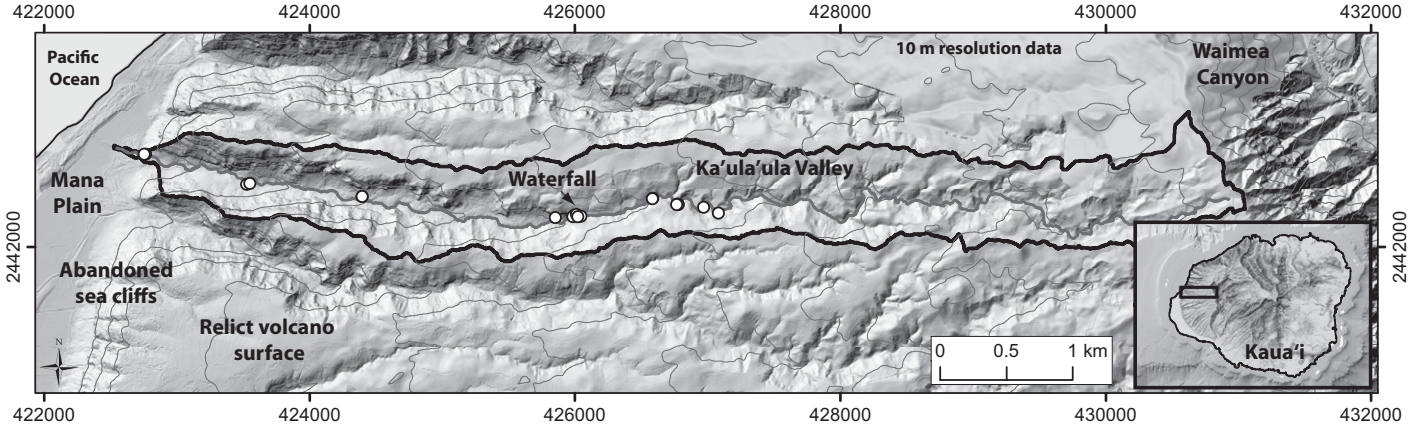

Figure 2. Shaded relief map of western Kaua'i generated from 2-m-resolution light detection and ranging (LiDAR) data (with a patch of 10-m-resolution data in the northeast corner). Ka'ula'ula Valley is outlined in black. The ephemeral Ka'ula'ula stream is highlighted in gray. The contour interval is 100 m. Cosmogenic sample locations are represented by white dots. Coordinates are UTM zone 4N. Inset shows overview of Kaua'i with location of Ka'ula'ula Valley indicated by box. LiDAR data are from the National Center for Airborne Laser Mapping collected in 2012.

(Fig. 4). In contrast, purely vertical incision (in the absence of propagating knickpoints) should generate cosmogenic nuclide concentrations that are a function of vertical incision rates. In this latter example, faster erosion rates will result in lower nuclide concentrations in the downstream section of the valley, due to the greater depth of incision (Fig. 4B).

Using a combination of both stable and radioactive cosmogenic nuclide isotope systems (^{3}He, ^{21}Ne, ^{10}Be, ^{26}Al, ^{36}Cl), Seidl et al. (1997) argued for knickpoint retreat as the dominant control on the evolution of Ka'ula'ula Valley. Of note, they used a 20,000 yr ^{26}Al exposure age of a cliff face 20 m downstream of the waterfall to calculate a waterfall retreat rate of ~1 mm/yr. This rate is similar to a long-term average waterfall migration rate assuming the knickpoint formed near the modern coastline and initiated ca. 4 Ma near the end of the shield-building stage, when the island was most susceptible to large-scale flank collapse. However, the cosmogenic exposure data of Seidl (1993) and Seidl et al. (1997) are not internally consistent in that different isotopic analyses produced significantly different accumulation ages for the same sample. Consequently, these data cannot definitively distinguish between the competing hypotheses of vertical incision and knickpoint propagation, or confidently establish long-term propagation rates. Since the study of Seidl et al. (1997), cosmogenic exposure dating methodology and constraints on production rates have greatly improved, notably for the use of cosmogenic ^{3}He in olivine (e.g., Licciardi et al., 1999; Dunai and Wijbrans, 2000; Gayer et al., 2008; Amidon et al., 2009; Fenton et al., 2009; Gillen et al., 2010; Goehring et al., 2010).

Field Methods and Sampling Strategy

To constrain the rates of channel incision and knickpoint retreat in Ka'ula'ula Valley, we took rock surface samples in order to measure the concentrations of cosmogenic ^{3}He within olivine phenocrysts in basalt. Sampling rock involved chipping off surface samples (~3 cm thick) with a hammer and chisel. We obtained samples along much of the channel, although access was limited in the upper reaches of the valley. We recorded the location and elevation of each sample via hand-held global positioning system (GPS) units. Due to the narrow geometry of the valley and nonhorizontal sample surfaces, we took topographic shielding correction measurements, including attitude of the sample face and skyline shielding (Balco et al., 2008).

Following the conceptual model of Seidl et al. (1997), we used different sampling strategies upstream and downstream of the waterfall to test the hypothesis of waterfall retreat based on the accumulation of cosmogenic isotopes (Fig. 4). Downstream of the waterfall, we targeted sites that appeared to have been emplaced shortly after the passage of the knickpoint, such as large boulders on talus-covered terraces, stable cliff faces, and abandoned bedrock strath surfaces well removed from the active channel (Fig. 2; Tables 1 and 2). The hypothesis is that nuclide concentrations of these features may record surface exposure ages, and a downstream trend in exposure age can be used to constrain waterfall retreat rate (Fig. 4). As described by Seidl et al. (1997), abandoned talus-covered terraces are preserved on both sides of the active channel and are mantled with 2–3 m angular, lichen-covered boulders, possibly emplaced by cliff collapse shortly after knickpoint passage when valley walls were near vertical (as seen in the modern inner gorge below the waterfall discussed later herein). These boulders show no evidence of fluvial reworking, significant erosion, or modification subsequent to emplacement.

Upstream of the waterfall, most samples were taken from bedrock and large boulders in and near the active channel (Table 1). The hypothesis here is that nuclide concentrations record the rate of steady vertical incision into bedrock or the boulder mantle (Fig. 4). Abandoned transport surfaces (e.g., terraces) are rare upstream of the waterfall, but we did collect a sample from one strath terrace located just upstream of the waterfall and 4 m above the active channel. We interpret nuclide concentration in this sample alone as a surface exposure age, which, combined with its local elevation, provides an additional constraint, independent of in-channel samples, on the rate of vertical incision. We also attempted to constrain the rates of incision using two samples of detrital olivine grains in sand deposits within the active channel (e.g., Gayer et al., 2008): The first was located just upstream of the waterfall and the second was at the mouth of the channel.

To correct for noncosmogenic sources of ^{3}He in the samples, we obtained a sample of basalt from within an irrigation tunnel that had been completely shielded from cosmic rays (>100 m below ground surface). This sample was taken from a ridge in eastern Hanalei Valley (~20 km to the southwest; Fig. 1) in the same rock formation (Waimea Group). We also incorporated and re-analyzed the raw helium data from Seidl (1993) to augment our samples

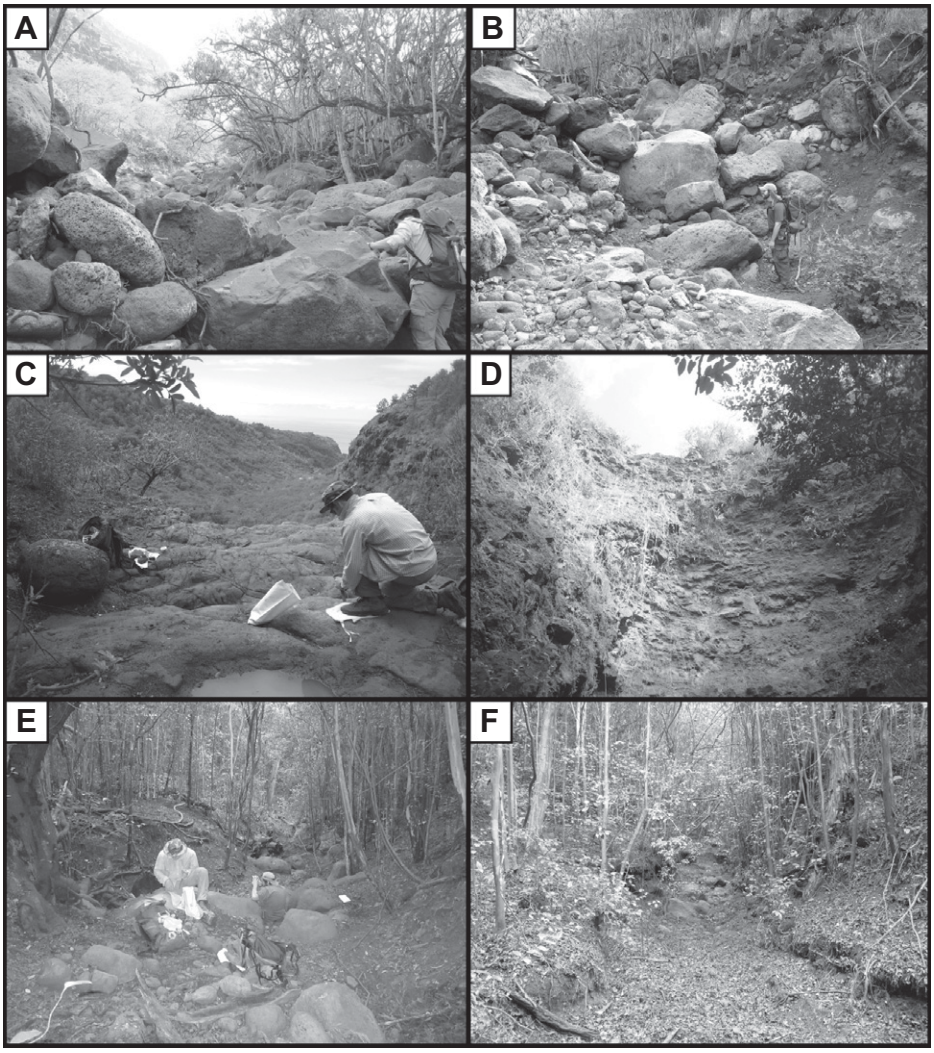

Figure 3. Photographs of Ka'ula'ula Valley. (A–B) Channel downstream of the waterfall showing large boulders (up to 2 m diameter) likely transported by debris flows. Note people for scale. (C) Sampling on the waterfall lip looking downstream within Ka'ula'ula Valley. (D) View up the 40-m-tall vertical waterfall face. (E) Sampling boulders in a section of channel above the waterfall. (F) View of the channel upstream from the waterfall; channel width is ~3 m.

(Table 2) and recalculated exposure ages based on the shielded-sample correction strategy we adopt here.

Sample Preparation and Age Measurements

We crushed the basalt samples with a jaw crusher and isolated olivine in the 1–4-mm-diameter fraction using hand magnets and hand-picking. Olivine samples were sonicated in 5% 2:1 HF:HNO_3 acid for ~1 h to remove any surface alteration, and phenocrysts were inspected to remove any with adhering groundmass. We ground each olivine sample, wet sieved the ground olivine to <37 μm, and allocated ~0.4 g per sample. Samples were heated in vacuum to 1300 °C, and the released ^{3}He and ^{4}He gas was analyzed on a MAP 215–50 noble gas mass spectrometer at the Caltech Noble Gas Laboratory (following Amidon and Farley, 2011). Cosmogenic ^{3}He production rates and accumulation ages were calculated using the CRONOS ^{3}He exposure age calculator following the scaling scheme of Lal (1991) and Stone (2000). Given the fact that we are primarily concerned with relative differences between samples in a small catchment, uncertainties in scaling and production rates are less important here than for studies spanning a large geographic range. Production rates for catchment-averaged samples were determined by calculating the latitude- and elevation-dependent production rate at each pixel of the upslope contributing digital elevation model (DEM) (e.g., DiBiase et al., 2010).

Helium concentrations in olivine phenocrysts include multiple components that must be isolated to quantify the cosmogenic ^{3}He component. The helium concentrations measured by fusion of olivine samples are governed by

$$^3\mathrm{He} = {}^3\mathrm{He}_c + [{}^3\mathrm{He}_m + {}^3\mathrm{He}_r], \quad (1)$$

$$^4\mathrm{He} = [{}^4\mathrm{He}_m + {}^4\mathrm{He}_r], \quad (2)$$

where He_c refers to cosmogenic He, He_m refers to mantle helium trapped in fluid and/or melt inclusions, and He_r refers to helium produced by radioactive decay and associated neutron capture on ^{6}Li (Aldrich and Nier, 1948; Morrison and Pine, 1955; Andrews and Kay, 1982; Lal, 1987). The brackets group "background" components, which are present even in cosmic ray–shielded samples.

The traditional approach to isolate the cosmogenic component is to assume that any measured ^{4}He is ^4He_m sourced from melt inclusions (Craig and Poreda, 1986; Kurz, 1986). However, for samples from older rock, as is the case here, ^4He_r cannot be neglected (Blard and Farley, 2008), and instead we used a shielded sample to estimate the background components (e.g., Cerling and Craig, 1994; Gosse and Phillips, 2001; Lifton et al., 2001; Margerison et al., 2005; Amidon and Farley, 2011). The components of ^{3}He can then be described by

$$^3\mathrm{He} = {}^3\mathrm{He}_c + {}^3\mathrm{He}_s, \quad (3)$$

where ^3He_s is the concentration of ^{3}He measured in a cosmic ray–shielded olivine sample (i.e., the bracketed terms in Eq. 1).

The shielded-sample approach assumes that the residual mantle ^{3}He concentration in the olivine is the same among exposed and shielded samples, which may not be the case. However, by precrushing the olivine to a fine grain size prior to analysis, the mantle component contained in melt or fluid inclusions is largely removed (Kurz, 1986). In addition, the shielded sample after crushing had a very low ^{3}He concentration of 0.04 M at/g (6% of our lowest measured ^{3}He cosmogenic concentration), indicating minimal residual ^{3}He in these samples. The shielded-sample approach assumes that the Li-produced ^{3}He is the same in shielded and exposed samples, which may only be valid if the samples all have the same chemistry and eruption age. However, Gayer et al. (2008) showed for Kaua'i rocks that even order-of-magnitude

TABLE 1. ^{3}He AND ^{4}He CONCENTRATIONS MEASURED DURING FUSION OF OLIVINE

Sample	Mass (g)	$[^3He]_{melt}$ (×10^6 at/g)	±1σ	$[^4He]_{melt}$ (×10^{12} at/g)	±1σ	$(^3He/^4He)_{melt}$ (R/R_A)
Shield	0.4082	0.04	0.004	0.016	0.002	1.6
KVW-01A	0.3675	1.24	0.07	0.026	0.003	33.9
KVW-01B	0.50975	0.67	0.04	0.013	0.001	35.9
KVW-02	0.42512	0.81	0.05	0.051	0.005	11.5
KVW-03	0.3651	2.27	0.14	0.166	0.017	9.9
KVW-04	0.47427	2.63	0.16	0.031	0.003	60.4
KVW-05	0.48643	2.10	0.13	0.029	0.003	51.8
KVW-07	0.5796	6.75	0.40	0.080	0.008	60.9
KVW-08	0.5191	9.74	0.58	0.112	0.011	62.7
KVW-09	0.3451	3.10	0.19	0.021	0.002	104.3
KVW-11	0.25002	2.28	0.14	0.034	0.003	47.7
KVW-12	0.54916	15.05	0.90	0.042	0.004	258.5
KVW-14	0.5964	2.13	0.13	0.037	0.004	41.3
KVW-15	0.40988	0.93	0.06	0.039	0.004	16.9
KVW-17	0.4497	2.19	0.13	0.018	0.002	87.1
KVW-18	0.47123	0.70	0.04	0.019	0.002	26.7
KVW-19	0.3648	3.57	0.21	0.148	0.015	17.3

Note: Analytical error is assessed at 6% based on repeat measurement of replicate samples (Amidon et al., 2009) with similar ^{3}He counting rates to this study (5–10 counts per second [cps]). Shielded sample has analytical error of 10% due to lower ^{3}He counting rates (<1 cps). R/R_A is the measured He isotope ratio divided by the atmospheric He isotope ratio (R_A), 1.4 × 10^{-6}.

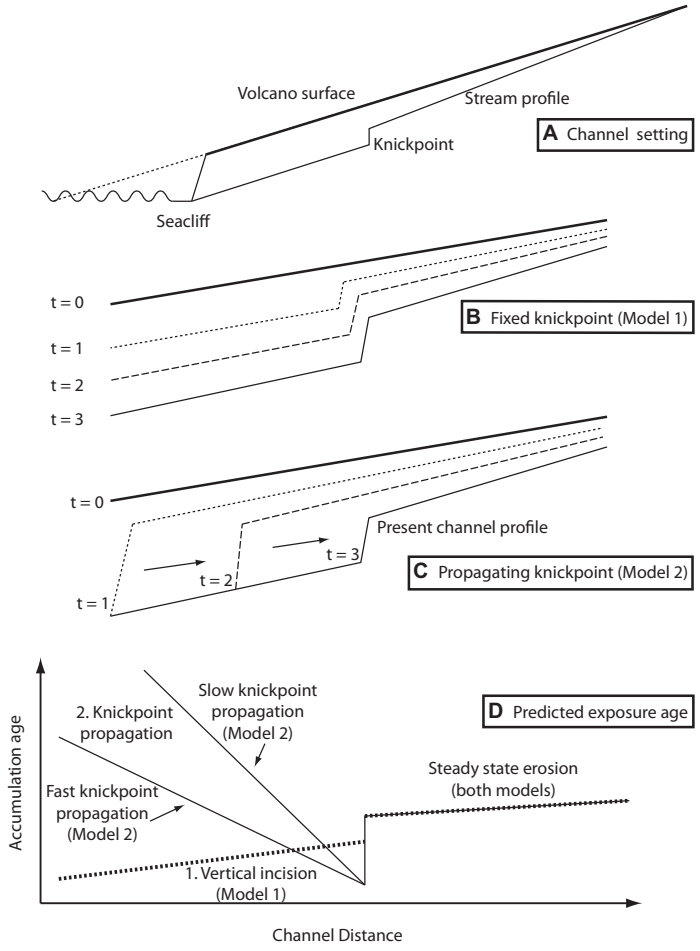

Figure 4. (A) Schematic of channel incising into the volcano surface with a prominent knickpoint midway up the channel. (B) Schematic of channel evolution assuming a fixed knickpoint and pure vertical incision (model 1). Lines represent channel elevation through time. (C) Illustration of channel evolution with an upstream-propagating knickpoint (model 2). (D) Predicted cosmogenic accumulation ages for the hypotheses represented in C and D. Slower migration rates generate older accumulation ages at the downstream end of the valley. Figure is modified from Seidl et al. (1997).

variations in chemical composition between shielded and exposed samples would have little impact on this correction. Therefore, the background ^{3}He from the shielded sample was subtracted from each sample (Table 2), following Equations 1 and 3, and the resulting concentrations of ^3He_c in olivine range from 0.67 to 15.05 M at/g (Table 2).

Our treatment of ^{3}He concentrations measured in olivine differed from that of Seidl et al. (1997), who used step-heating to melt the phenocrysts and corrected for mantle-derived ^{3}He assuming a minimum R/R_A of 8 (R/R_A is measured ^{3}He/^{4}He divided by ^{3}He/^{4}He ratio in the atmosphere, 1.4 × 10^{-6}). Given the potential for significant ingrowth of ^4He_r and the high ^3He_m measured in Kaua‘i olivine (mean R/R_A of ~24; Gayer et al., 2008), we argue that our approach of thoroughly crushing the sample prior to heating, and using a shielded sample to correct for non-cosmogenic sources of ^{3}He is better suited to this site. Therefore, we re-analyzed the raw data from Seidl (1993) and Seidl et al. (1997) with the same correction procedure used for our samples. We measured olivine from the same locations as Seidl (1993) in cases by relocating drill holes, and the results are generally comparable (e.g., see KVW-11 and KCKP, Table 2).

Cosmogenic ^{3}He Results

Cosmogenic data are presented in Tables 1 and 2 and are shown in Figure 5. Cosmogenic accumulation ages downstream of the waterfall are greatest near the valley mouth (KVW-8, 120 ka), and decrease upstream (Fig. 5; Table 2). A boulder sampled on a talus-covered terrace ~1 km upstream of the mouth has an age of ca. 80 ka (KVW-7), similar to a boulder sampled by Seidl (1993) in this vicinity (K560, 81 ka). Two adjacent boulders located ~2 km upstream from the stream mouth (KVW-4 and 5) have exposure ages of 22 ka and 27 ka. KVW-3, a small cliff exposure 150 m downstream of the waterfall has an age of 27 ka, and two samples taken from a cliff 20 m downstream of the waterfall have ages of 9 ka and 18 ka (KVW-1A, KVW-1B). A large boulder in the channel 40 m downstream of the waterfall has an age of 8 ka (KVW-2). Together, these samples indicate progressively younger accumulation ages from the valley outlet to the waterfall, and if interpreted as surface exposure ages, they are consistent with knickpoint retreat (Fig. 4).

The bedrock riverbed at the lip of the waterfall (KVW-11, Fig. 3C) has an accumulation age of 20 ka (Table 2). We interpret this accumulation age in terms of a vertical erosion rate (rather than a surface exposure age) because it is within the actively eroding channel, which yields

TABLE 2. SAMPLE LOCATIONS AND ^{3}He EXPOSURE AGE

Sample	Description	Distance (m)	Lat (°N)	Long (°W)	Elevation (m)	Topo shield	$[^3He]_{melt}$ ($\times10^6$ at/g)	^{3}He prod rate (at/g/yr)	Exposure age (yr)	±1σ
KVW-1A	Cliff exposure	6541	22.0833	159.7177	512	0.55	1.20	68	1.8E+04	1.4E+03
KVW-1B	Cliff exposure	6541	22.0833	159.7177	513	0.55	0.63	68	9.3E+03	7.4E+02
KVW-02	Channel boulder	6551	22.0832	159.7177	510	0.75	0.78	92	8.5E+03	6.7E+02
KVW-03	Cliff exposure	6696	22.0833	159.7188	503	0.70	2.24	83	2.7E+04	2.1E+03
KVW-04	Terrace boulder	8412	22.0847	159.7329	298	0.93	2.60	95	2.7E+04	2.1E+03
KVW-05	Terrace boulder	8412	22.0847	159.7329	298	0.93	2.07	95	2.2E+04	1.7E+03
KVW-07	Terrace boulder	9387	22.0854	159.7413	168	0.91	6.71	82	8.2E+04	6.3E+03
KVW-08	Bedrock strath	10,314	22.0875	159.7487	40	0.98	9.71	83	1.2E+05	9.2E+03
KVW-09	Channel sand	10,324	22.0875	159.7488	36	Catch	3.06	123	2.5E+04	1.9E+03
KVW-11	Channel bedrock	6511	22.0834	159.7171	554	0.90	2.24	110	2.0E+04	1.6E+03
KVW-12	Bedrock strath	6521	22.0835	159.7172	558	0.98	15.02	121	1.2E+05	9.7E+03
KVW-14	Channel boulder	5873	22.0847	159.7117	592	0.88	2.10	113	1.9E+04	1.4E+03
KVW-15	Channel boulder	5873	22.0847	159.7117	592	0.88	0.89	113	7.9E+03	6.2E+02
KVW-17	Terrace boulder	5342	22.0841	159.7081	632	0.95	2.16	125	1.7E+04	1.3E+03
KVW-18	Channel boulder	5151	22.0836	159.7068	640	0.93	0.67	123	5.4E+03	4.3E+02
KVW-19	Channel sand	6487	22.0834	159.7169	555	Catch	3.53	140	2.5E+04	1.9E+03
Samples from Seidl (1993)										
KCKP	Channel bedrock	6511	22.0834	159.7171	555	0.90	2.44	110	2.2E+04	2.5E+03
c2000	Channel bedrock	5636	22.0842	159.7098	612	0.90	1.98	116	1.7E+04	1.9E+03
K560	Terrace boulder	9357	22.0855	159.7411	169	0.90	6.71	83	8.1E+04	9.1E+03
KVBPT	Channel boulder	5622	22.0842	159.7098	612	0.90	1.48	116	1.3E+04	1.4E+03
KVBPT-B	Channel boulder	5636	22.0842	159.7099	611	0.90	1.70	116	1.5E+04	1.6E+03

Note: $[^3He]_{melt}$ has been corrected for ^{3}He measured in the shielded sample (Table 1). The lower panel of data was taken from Seidl (1993) and represents total ^{3}He released upon heating. Error was not specified, so we applied an analytical error of 10%. Topographic shielding is estimated at 0.9, and exposure age was calculated as per samples from this study. Distance refers to channel distance (Fig. 5). All samples include a thickness shielding correction of 0.976. Exposure age was calculated using the CRONUS ^{3}He calculator, and we used the Lal/Stone scaling equations. Exposure age error includes internal and external uncertainties.

0.027 mm/yr. This compares well to a sample (KCKP) taken in the same location by Seidl (1993) (Table 2), which we calculate to have an erosion rate of 0.025 mm/yr. The sole sample from a strath terrace near the waterfall has an accumulation age of 120 ka (KVW-12). The elevation difference between the waterfall lip and the nearby terrace is 4 m, and if we interpret the strath terrace accumulation age as a surface exposure age, we find a vertical incision rate of 0.03 mm/yr (i.e., 4 m/120 k.y.). If we use the accumulation age at the eroding waterfall lip as an estimate of inheritance prior to abandonment, then the terrace sample yields an incision rate of 0.025 mm/yr (i.e., 4 m/100 k.y.). As noted by Seidl et al. (1997), the rate of vertical erosion at the waterfall lip is similar to the long-term vertical incision rate (0.02 mm/yr) assuming a 4 Ma original volcano surface, and taking into account the observed 80 m of relief between the modern channel floor and the relict volcanic surface. Thus, despite uncertainty in some of the assumptions, multiple methods converge to a vertical incision rate just upstream of the waterfall lip of ~0.02–0.03 mm/yr.

Upstream of the waterfall, the samples of bedrock and large boulders within 1 km of the waterfall have accumulation ages ranging from 5 to 19 ka (samples KVW-14, 15, 17, 18). Bedrock accumulation ages are generally older than boulder samples (Fig. 5), likely because boulders may have entered the channel at any time, and they are likely derived from deep-seated failures with little inheritance. Young ages might also reflect a recent pulse of erosion related to the 10-m-high knickpoint ~2.5 km upstream of the primary waterfall (Fig. 6A), which we were unable to access in the field. If interpreted as reflecting steady-state vertical incision (Seidl et al., 1997), these measurements indicate incision rates ranging from 0.029 to 0.11 mm/yr, with the lower values consistent with the measured rates at the waterfall lip. These erosion rates are also consistent with inferred rates measured from detrital olivine samples from the active channel, which yielded identical erosion rates at the valley mouth and at the waterfall lip of 0.022 mm/yr.

Testing Conceptual Models of Vertical Incision and Knickpoint Retreat

To compare our accumulation age data with theoretical predictions along the valley transect proposed by Seidl et al. (1997) (Fig. 4), we modeled the expected distribution of accumulation ages based on competing ideas of the evolution of Ka'ula'ula Valley. The model end members are (1) constant vertical incision with a fixed knickpoint location (Fig. 4B) (cf. Kirby and Whipple, 2012), and (2) knickpoint retreat initiated at two different times, 4 Ma and 120 ka. These times respectively reflect knickpoint initiation shortly after island formation, and initiation at the time of our oldest downstream exposure age.

Pure vertical erosion without knickpoint migration assumes that nuclide accumulation is dependent on depth of incision and volcano age, so that the accumulation age is $t = \Lambda/E$. We calculated E as the average erosion rate needed to incise from the original volcano surface to the present channel floor over a total duration of 4 m.y. We approximated the original shield volcano surface by fitting a seventh-order polynomial surface to the broad, relict volcanic surfaces preserved as interfluves bounding Ka'ula'ula Valley (Fig. 2; sensu Ferrier et al., 2013a). This exercise results in an approximately uniform erosion rate of ~0.025 mm/yr upstream of the knickpoint, equating to an accumulation age of ca. 22 ka (Fig. 5). The accumulation age systematically decreases as the greater incision depth toward the valley outlet requires more rapid mean erosion rates.

The scenario of spatially uniform exposure ages is compatible with the measurements upstream of the waterfall, but it is incompatible with measurements downstream of the waterfall. Upstream of the waterfall, the accumulation ages are scattered, but they are generally consistent with the hypothesis of constant vertical incision, at least for the time scale over which the cosmogenic concentrations are averaged (tens of thousands of years). Nevertheless, the model predictions for the case of constant vertical incision are slightly older than the exposure age measurements (Fig. 5), which may reflect greater incision rates over the past 5–20 k.y. as compared to over the entire posteruptive history of the volcano (~4 m.y.) (e.g., due to the 10-m-high knickpoint ~2.5 km upstream of the primary waterfall), or spatially nonuniform erosion or landslides working through the catchment. Alternatively, the rates may be reconciled by allowing for some slow rate of surface lowering of the relict volcanic surfaces via soil formation. For example, a net interfluve lowering rate

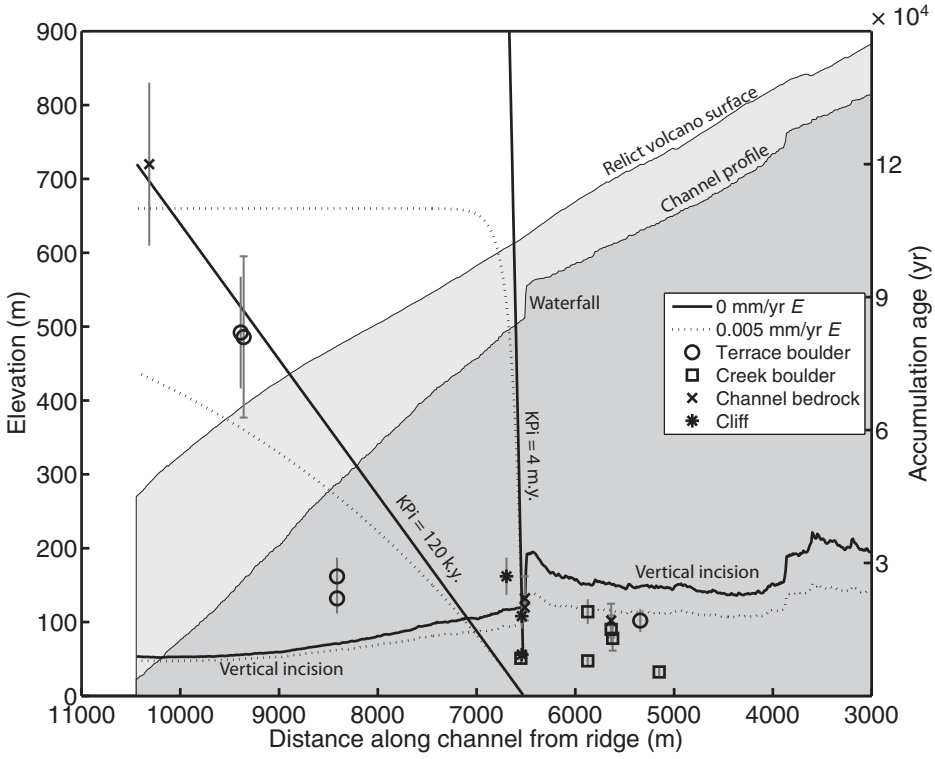

Figure 5. Topographic profile of the channel bed and the relict volcano surface that borders Ka'ula'ula Valley, measured cosmogenic accumulation ages (symbols), expected cosmogenic accumulation ages for pure vertical incision upstream of the waterfall, and the following scenarios for downstream of the waterfall: pure vertical incision, knickpoint initiation (KPi) at the coast at 120 ka, and knickpoint initiation at the coast at 4 Ma (thick solid lines). Solid lines assume no background erosion, whereas dashed lines represent the expected accumulation ages given erosion (*E*) of the surface following passage of the knickpoint at a rate of 0.005 mm/yr. All distances are channel distance measured from the topographic divide (ridge) at the headwaters of Ka'ula'ula Valley. Only samples taken from terraces downstream of the waterfall and the active channel upstream of the waterfall are shown (e.g., detrital samples are not shown) to aid comparison with model expectations. Error bars with small horizontal ticks indicate samples from Seidl (1993). The channel profile was extracted from the 2-m-resolution light detection and ranging (LiDAR) data set along the path of steepest descent extracted from a down-sampled 10 m digital elevation model to avoid routing flow within sub-channel-width roughness (e.g., Snyder, 2009).

of 0.005 mm/yr (equivalent to 20 m over 4 m.y.) would place ages inferred from the relief and age of the valley in line with our oldest cosmogenic exposure measurements upstream of the waterfall (Fig. 5). Other mechanisms that may explain this discrepancy that we cannot rule out include intermittent burial by alluvium, or self-shielding if periodically mobile boulders were resting on different faces (Mackey and Lamb, 2013).

Rather than vertical channel incision astride an immobile waterfall, an alternative hypothesis to explain the exposure ages of terraces downstream of the waterfall is progressive abandonment during knickpoint retreat (Figs. 4–5; Seidl et al., 1994, 1997). We calculated the expected accumulation age of abandoned terraces by assuming no inheritance prior to abandonment. Our exposure data show a trend of increasing age downstream of the waterfall, but we would expect much older exposure ages for the case of knickpoint initiation by flank collapse ca. 4 Ma (Seidl et al., 1997).

Erosion of boulders on terraces following passage of the knickpoint would modify the accumulation ages, and we explored whether this could explain the discrepancy between our measured accumulation ages and those expected for knickpoint initiation at 4 Ma. The nonfluvial background erosion rate is unconstrained; however, as noted already, a nonfluvial erosion rate of 0.005 mm/yr applied to the interfluves would bring expected accumulation ages from the interfluve and channel-bed topography in line with our accumulation age measurements upstream of the waterfall. Application of this inferred erosion rate to the terrace samples results in accumulation ages that should be spatially uniform at just over 100 ka, inconsistent with the data (Fig. 5), and no reasonable value of background erosion can reconcile the discrepancy between our cosmogenic measurements and the model for knickpoint initiation at 4 Ma. Moreover, the sampled bedrock and boulders on terraces are angular, hard, and appear minimally weathered. Boulders that have eroded sufficiently to reach a steady-state erosion rate would have a smooth rounded surface, reflecting radial erosion equating to at least several e-folding lengthscales of cosmic-ray penetration (Mackey and Lamb, 2013).

Because we sampled boulders on debris terraces adjacent to the stream, it is possible that they rolled into position via cliff collapse at some time unrelated to passage of the knickpoint. For example, the samples at 8.4 km have an exposure age younger than that predicted by the trend of knickpoint retreat (Fig. 5), and so they potentially fell into place sometime after the waterfall passed. If pervasive, this mechanism is likely to produce random ages, and it is not compatible with the accumulation ages systematically increasing downstream from the waterfall. Similarly, any cosmogenic inheritance the boulders may have had prior to deposition (e.g., while on a cliff face) would likely generate a random distribution of ages, inconsistent with our measurements.

Our preferred interpretation of the ^{3}He exposure data is that the knickpoint was initiated at ca. 120 ka, coincident with our downstream-most accumulation age. Since initiation, the knickpoint appears to have propagated steadily upstream, leaving boulders abandoned on terraces that have been minimally affected by postdepositional erosion (and therefore the accumulation ages represent approximate surface exposure ages). This interpretation requires the knickpoint to have migrated ~4 km over ~120 k.y., equating to an average retreat rate of 33 mm/yr.

WATERFALL EROSION PROCESSES AND MODELING

The waterfall headwall in Ka'ula'ula Valley is a single vertical step and is composed of multiple basalt flows that are blocky and jointed at the decimeter to meter scale (Fig. 3D). Most models for waterfall retreat, many of which have been applied to this site, assume that waterfall retreat is governed by fluvial incision processes acting on the face of the waterfall headwall. These models include stream power (e.g., Seidl et al., 1994; Stock and Montgomery,

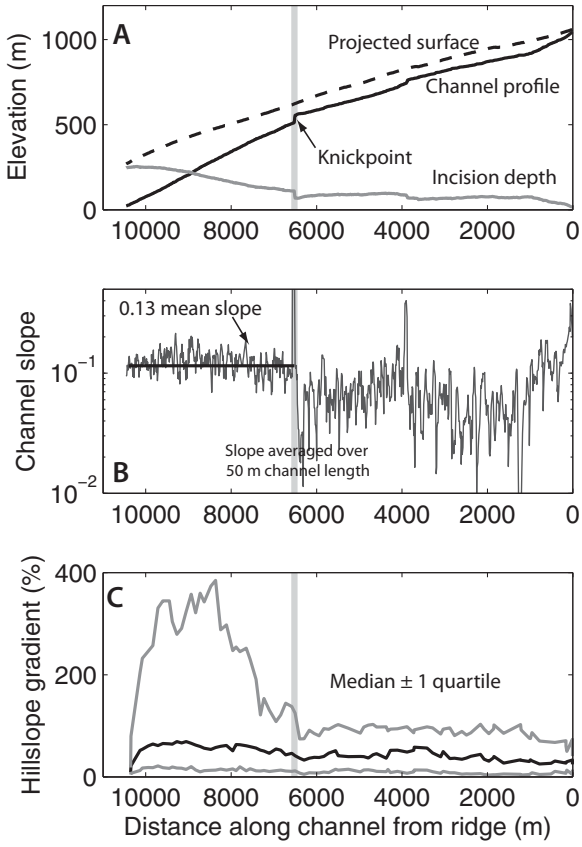

Figure 6. Valley response to knickpoint retreat measured from 2-m-resolution light detection and ranging (LiDAR)–derived topography. (A) Channel longitudinal profile with projected original surface, and depth of incision. Waterfall location in all figures is marked by the vertical gray band. All distances are measured from the topographic divide (ridge) at the headwaters of Ka'ula'ula Valley. (B) Channel slope averaged over 50 m of channel length. The slope is systematically higher downstream of the knickpoint (13%) compared to upstream (~8%). (C) Median hillslope gradient (±1 quartile) along the valley determined every 100 m.

1999; DeYoung, 2000) and saltation-abrasion (Chatanantavet and Parker, 2005). The waterfall face, however, shows no indicators of active abrasion (e.g., smooth sculpted rock, flutes, or potholes; the waterfall was dry during our field campaign) (Fig. 3D). Moreover, given the vertical headwall, we suspect that it is highly likely that flow detaches from the waterfall face, and so the stream power and saltation-abrasion models would be inappropriate for the erosional mechanics of this knickpoint (e.g., stream power predicts infinite erosion rates for vertical steps). Vertical drilling of multiple steps has been advocated as a waterfall erosion mechanism elsewhere on the Hawai'ian islands (Howard et al., 1994; Lamb et al., 2007), but the waterfall face of Ka'ula'ula Valley is composed of a single vertical step with no successions of plunge pools (Figs. 3C and 5).

The remaining documented waterfall erosion mechanisms include undercutting within a plunge pool or toppling of jointed rock. Undercutting is the dominant waterfall retreat mechanism in many landscapes, especially where there exists a strong-over-weak stratigraphy (e.g., Gilbert, 1890; Lamb et al., 2006; Haviv et al., 2010). However, for the case of Ka'ula'ula Valley, despite the obvious layering of basalt flows, we note no obvious differences in rock strength, and the headwall lacks overhangs or undercutting. In addition, there is no plunge pool at the base of the waterfall, although bedrock is not exposed at the waterfall base, and we cannot rule out the possibility that a plunge pool exists and is filled with debris. This notwithstanding, significant burial is unlikely because there is no talus slope or debris apron abutting the waterfall escarpment. Our favored waterfall retreat mechanism is toppling of jointed rock, which is consistent with observations of waterfalls in jointed rock in other locations (Weissel and Seidl, 1997; Crosby and Whipple, 2006; Lamb and Dietrich, 2009). Although models have been developed for the threshold to initiate toppling (Lamb and Dietrich, 2009), the waterfall propagation rate in this case may depend on the ability of the flow to export collapsed material away from the headwall (Lamb et al., 2008).

Besides stream power, the most common knickpoint retreat models are those that seek a positive power-law correlation with drainage area (a proxy for water discharge; e.g., Rosenbloom and Anderson, 1994; Crosby and Whipple, 2006; Berlin and Anderson, 2007). However, some studies have found no drainage area dependence (Seidl et al., 1996; Weissel and Seidl, 1998; Cook et al., 2013) or even an inverse relationship between retreat rate and drainage area (Jansen et al., 2011).We examined the ability of drainage area–dependent waterfall-retreat models to reproduce observed cosmogenic accumulation ages using

$$\frac{dx}{dt} = cA^p, \tag{4}$$

where dx/dt is the upstream retreat rate, A is the upstream drainage area, and c (units of length $^{(1-2p)}$/time) and p (unitless) are fit constants. We explored the ability of Equation 4 to match our cosmogenic accumulation ages with a variety of c and p values and waterfall initiation ages, under the constraint that models must accurately predict the location of the present waterfall within 100 m. We evaluated performance based on the residual sum of squares (RSS) between model predicted time for the location of the knickpoint and the time measured by our cosmogenic accumulation ages for the same location (sensu Stock and Montgomery, 1999; Crosby and Whipple, 2006; Berlin and Anderson, 2007). Previous workers have suggested different c and p values for different sites that include both waterfalls and slope-break knickpoints (e.g., Rosenbloom and Anderson, 1994; Crosby and Whipple, 2006; Berlin and Anderson, 2007), none of which fits the data for Ka'ula'ula Valley. Instead, we find statistically good fits can be found with a variety of c and p values. For example, setting $p = -3$, $p = 0$, and $p = 1$ and solving for the best-fit value of c (2.7×10^{18} m^7/yr, 3.7×10^{-2} m/yr, 9.4×10^{-9} m^{-1}/yr, respectively) and knickpoint initiation time (118 ka, 102 ka, and 94 ka, respectively) all yield similar RSS values (1.1×10^9 yr, 2.2×10^9 yr, and 2.8×10^9 yr, respectively; Fig. 7). Despite the uncertainty in the exact model parameter values, the simplest explanation of our data remains a constant rate of knickpoint retreat (i.e., $p = 0$), but we cannot definitively rule out either positive or negative dependencies on drainage area.

LANDSCAPE RESPONSE TO KNICKPOINT RETREAT

How hillslopes and channels respond to knickpoint retreat is a fundamental question in landscape evolution, as it determines the rate at which changes in base level will be transmitted through the landscape (e.g., Korup and Schlunegger, 2007; Reinhardt et al., 2007; Gallen et al., 2011). The passage of a knickpoint presents a transient case whereby we can observe the along-channel behavior of hillslopes and compare hillslope properties pre- and post-knickpoint. When knickpoint propagation speed is known, along-channel distance can be transformed into time-since-knickpoint passage to

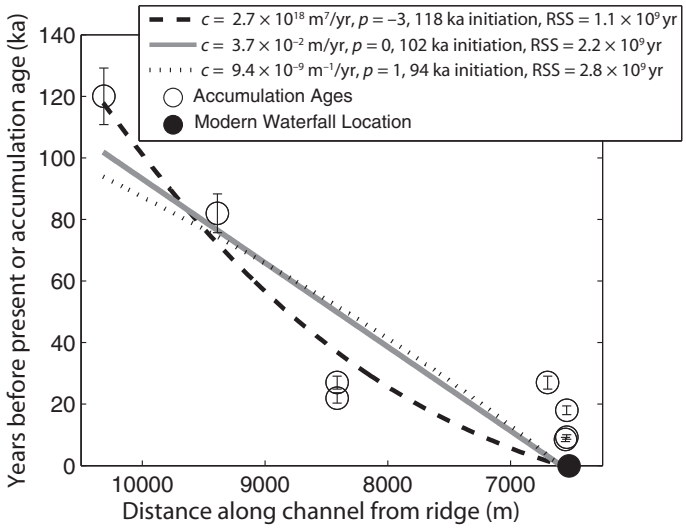

Figure 7. Comparison of a knickpoint retreat model (Eq. 4) with measurements of accumulation ages downstream of the modern waterfall location. Lines show combinations of *c*, *p*, and knickpoint initiation time that yield reasonable fits to the cosmogenic accumulation ages assuming an accumulation age of zero at the active waterfall. All distances are measured from the topographic divide (ridge) at the headwaters of Ka'ula'ula Valley. Drainage area was calculated from 10-m-resolution light detection and ranging (LiDAR) data. Modeling followed standard procedures outlined in Crosby and Whipple (2006) and Berlin and Anderson (2007). RSS—residual sum of squares.

constrain the rate of hillslope response. Importantly, hillslope response serves as a test for our inferred rapid rate of knickpoint propagation, because a slow or immobile knickpoint (e.g., due to a resistant rock unit) may not cause systematic changes to hillslopes in the downstream direction. In this section, we quantify the valley topography to assess how the passage of the knickpoint affected Ka'ula'ula Valley. We present field and topographic analysis and assess the hillslope response time.

While sampling for cosmogenic exposure ages, we documented the character of the channel and adjacent hillslopes. To augment these field observations, we performed topographic analysis of the region using a LiDAR data set resampled to 2 m resolution. We divided the valley into 100-m-wide north-south–oriented swaths spanning the width of the valley and calculated the statistics of topography within each swath. Topographic analysis revealed two contrasting geomorphic domains, separated by the waterfall located 4 km upstream from the valley outlet (Fig. 6). The boulder-lined channel axis below the knickpoint is nearly straight in planform, has a consistent channel-bed gradient (~13%), and is confined to a narrow valley with steep (sometimes vertical) rocky walls. The median slope of the valley downstream of the waterfall is 56%, with a high proportion of very steep topography (Fig. 6C).

Large, >2-m-diameter boulders in the channel downstream of the knickpoint show evidence of active mobility and deposition from debris flows (Figs. 3A–3B) including matrix-supported and poorly sorted deposits, large boulder clusters with levee and snout morphologies (e.g., Whipple and Dunne, 1992), and boulders burying vegetation indicating active transport. Both the uniform slope of the channel and its steep gradient are consistent with debris flows as the dominant erosion and transport process (Stock and Dietrich, 2003, 2006). Seidl et al. (1997) proposed the mechanism of knickpoint propagation under a largely immobile boulder mantle, but our observations indicate a dynamic environment downstream of the knickpoint where boulders are actively moved. This is supported by the observation that large boulders dominate the bed morphology to the valley mouth, including a debris fan that debouches on the Mana Plain, indicating active boulder transport by debris flows during the Holocene.

In comparison to the channel reach downstream of the knickpoint, upstream of the knickpoint the average channel gradient is lower (~8%), bed sediment is finer (gravel and cobbles as compared to boulders; Figs. 3E–3F), and bed sediment is locally sorted into bars and pools, indicative of fluvial processes rather than debris flows. Occasional boulders are present in the upstream reach (Fig. 3E), but these are angular, lack evidence of fluvial transport, and appear to have rolled in from side slopes. In this region, hillslopes are soil mantled and vegetated, and they have a consistently lower median slope of 30%–40% (Fig. 6C) as compared to the extensive subvertical rocky cliffs downstream of the knickpoint. There is not a major difference in rock type upstream of the knickpoint as compared to downstream, which suggests that the steeper topography downstream is due to passage of the knickpoint itself.

Supporting evidence for active knickpoint migration comes from a prominent inner gorge with steep valley walls just downstream from the waterfall. Within the inner gorge, valley width increases from ~150 m to ~500 m within the first ~200 m downstream of the waterfall (Fig. 2). We extracted hillslope profiles perpendicular to the valley axis using the LiDAR data within 102 m downstream of the waterfall (Fig. 8). Assuming a knickpoint retreat rate of 33 mm/yr, these profiles correspond to up to 3100 yr since passage of the knickpoint. Profiles were normalized by distance and elevation with respect to the nearby active channel to aid in comparison. Evidence of the passing knickpoint can be seen in the lower ~50 m of relief above the channel floor, consistent with the waterfall height, where hillslopes are initially steep (~120%) and then relax toward the same gradient as the rest of the valley (~60%) (Fig. 8).

Hillslope or scarp evolution is often modeled as a diffusive process (Hanks, 2000). The Ka'ula'ula Valley hillslopes, however, are steep and show evidence for landslides, rockfall, and talus accumulation, and thus they are not likely responding in a diffusive manner (Roering et al., 1999). This notwithstanding, it is useful to derive an apparent diffusivity to compare the hillslope relaxation rates in Ka'ula'ula Valley with other studies. We limit our analysis to 102 m downstream of the modern waterfall, because hillslope profiles appear similar beyond this point, suggesting that the hillslopes have fully responded to the waterfall migration. We calculated a range of apparent diffusivities (k = 1.4–3.2 m^2/yr) using $k = \Delta x^2/\Delta t$, where $\Delta x \approx$ 65–100 m is a characteristic length scale of hillslope response based on observed hillslope profiles (Fig. 8), and $\Delta t \approx 3100$ yr is a characteristic time scale for that response, corresponding to the elapsed time inferred between our furthest upstream and furthest downstream profiles assuming constant knickpoint retreat

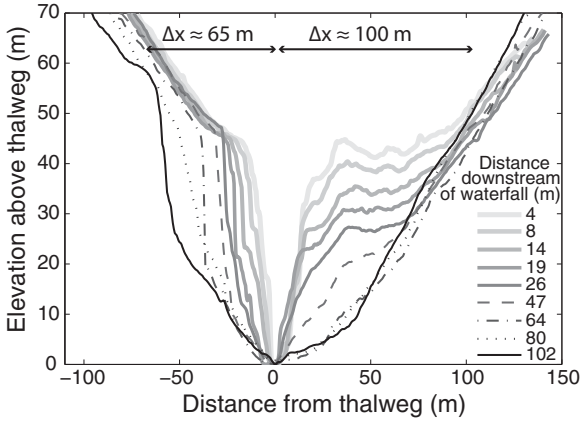

Figure 8. Hillslope profiles within 102 m downstream of the waterfall perpendicular to the channel axis. Profiles are plotted relative to the elevation of the local channel thalweg in order to allow for visual comparison among profiles at different absolute elevations. Double-arrowed lines show estimates of hillslope relaxation length (Δx) used in apparent diffusivity calculations.

of 33 mm/yr (Fig. 8). A diffusivity approaching 3 m^2/yr is higher than many previously reported. For example, compilations of diffusivities for fault scarps, terraces, shorelines, and hillslopes show that k ranges from ~1 × 10^{-4} m^2/yr to ~2 × 10^{-2} m^2/yr, with areas of higher precipitation generally having higher values of k (Hanks, 2000). McKean et al. (1993) reported values as high as $k = 3.6 \pm 0.55$ m^2/yr for a soil-mantled hillslope near San Francisco, California. We suspect the high apparent diffusivities for Ka'ula'ula Valley result from rockfall and other mass-wasting processes being dominant rather than soil creep, in addition to transient high relief driven by rapid upstream propagation of the knickpoint. This analysis is also self-consistent with our interpretation (and that of Seidl et al., 1997) that the boulder debris on terraces is a relict from shortly after knickpoint retreat (i.e., within ~3 k.y.).

KNICKPOINT INITIATION

Previous studies along the Na Pali coast have proposed a common origin for both the sea cliffs and the initiation mechanism of steep knickpoints in many of the streams (e.g., Seidl et al., 1994, 1997; DeYoung, 2000). However, the primary process for sea-cliff formation is contested. Specifically, the formation of the high sea cliffs along the Na Pali coast has been attributed to both submarine landsliding (Hinds, 1930) and wave erosion (Stearns, 1985). Submarine flank collapse has been the favored mechanism of cliff formation along northern Kaua'i because of widespread submarine landslide debris (Moore et al., 1989), the slow cosmogenic-derived waterfall retreat rate (1 mm/yr) reported by Seidl et al. (1997), and the impressive knickpoints along the eastern Na Pali coast (~250 m of relief), which are approximately twice as high as any Quaternary sea-level fluctuations (Chatanantavet and Parker, 2005). Despite the appeal of the flank collapse hypothesis for knickpoint generation along the Na Pali coast, it has not been tested quantitatively, and our new knickpoint retreat rates bring this interpretation into question.

Knickpoint Formation by Submarine Landsliding?

To assess the potential for either submarine landslides or cliff erosion to generate the Na Pali coast cliffs, we used bathymetry (50 m horizontal resolution) surrounding Kaua'i to look for evidence of submarine landslides off the Na Pali coast and Mana Plain. The bathymetry off the coast of northwestern Kaua'i (Fig. 1) shows a gentle plain extending ~7 km offshore, to ~120 m depth (Fig. 9A). The seafloor then drops away relatively steeply to ~400 m depth, whereupon it continues at a gradual slope out to ~850 m depth. At ~850 m below sea level, the island flank drops away steeply, and this break in slope has been interpreted as the approximate shoreline of the island during formation, accounting for the different angles of lava solidification on land and under water (Mark and Moore, 1987; Flinders et al., 2010). This topographic profile has been interpreted to show modification of the original shield volcano surface, which can be reconstructed by projecting the relict volcano surface offshore (Fig. 9A) to align with the deeply submerged original flank of the volcano ~400 m below sea level (Inman et al., 1963). Well logs across the Mana Plain indicate up to 130 m of coralline sand and clay-rich lagoon sediments on top of an irregular gently dipping (~5°) basalt bedrock bench (Macdonald et al., 1960), suggesting deposition of sediment over a submerged wave-cut platform (Inman et al., 1963). Whole-rock amino acid dating of carbonate dunes on the Mana Plain indicates that they were deposited during the last interglacial (Hearty et al., 2000).

The gently sloping bathymetry off the northwestern Na Pali coast and the geometry of the Mana Plain show no morphologic evidence for a large submarine landslide (Fig. 1). Given the comparatively young age of knickpoint initiation suggested by our cosmogenic exposure dating (ca. 120 ka), we would expect to see clear evidence for a large failure in the bathymetry if the knickpoint was caused by flank collapse. The seafloor morphology does, however, show morphological evidence for a large flank collapse on the eastern Na Pali coast (Fig. 1), with an arcuate headscarp and debris field to the northeast (Moore et al., 1989). Therefore, the largest sea cliffs and some of the larger (~200 m) knickpoints within the eastern Na Pali coast channels may have been generated by submarine landsliding as advocated by previous studies. This mechanism, however, cannot explain the formation of the sea cliffs and knickpoints in Ka'ula'ula Valley and channels near the Mana Plain.

Knickpoint Formation by Sea-Cliff Erosion

In the absence of evidence for large submarine failure off the coast of northwestern Kaua'i near Ka'ula'ula Valley, we focus on sea-level–driven base-level change and wave cutting as the potential causes for cliff formation and knickpoint initiation. Changes in sea level have been widely documented to generate knickpoints, primarily during relative sea-level fall (e.g., Weissel and Seidl, 1998; Bishop et al., 2005; Crosby and Whipple, 2006; Loget and Van Den Driessche, 2009; Ye et al., 2013). Somewhat counterintuitively, sea-level highstands also have the potential for generating knickpoints via cliff erosion (Fig. 10). For example, if the rate of cliff erosion is faster than streams are able to incise vertically, and the channel is steeper than the shore platform generated by cliff erosion, then a knickpoint will be developed at the coast (e.g., Snyder et al., 2002). As an example, small coastal gullies in southern England are thought to have formed during rising sea level resulting in cliff erosion during the early Holocene (Leyland and Darby, 2008; Leyland and Darby, 2009), and a similar mechanism was proposed for Holocene cliffs in Tahiti (Ye et al., 2013). Similarly, Leckie (1994) reported that Holocene coastal erosion on New Zealand's eastern South Island caused the rivers to steepen and incise near the coast. Given the Na Pali coast's exposure to high-energy waves coming from the North Pacific swell and northeast trade winds, it is prone to significant coastal erosion (Inman et al., 1963; Vitousek and Fletcher, 2008). To evaluate this hypothesis, we constrain the relative sea-level history of Kaua'i and model cliff erosion by wave attack.

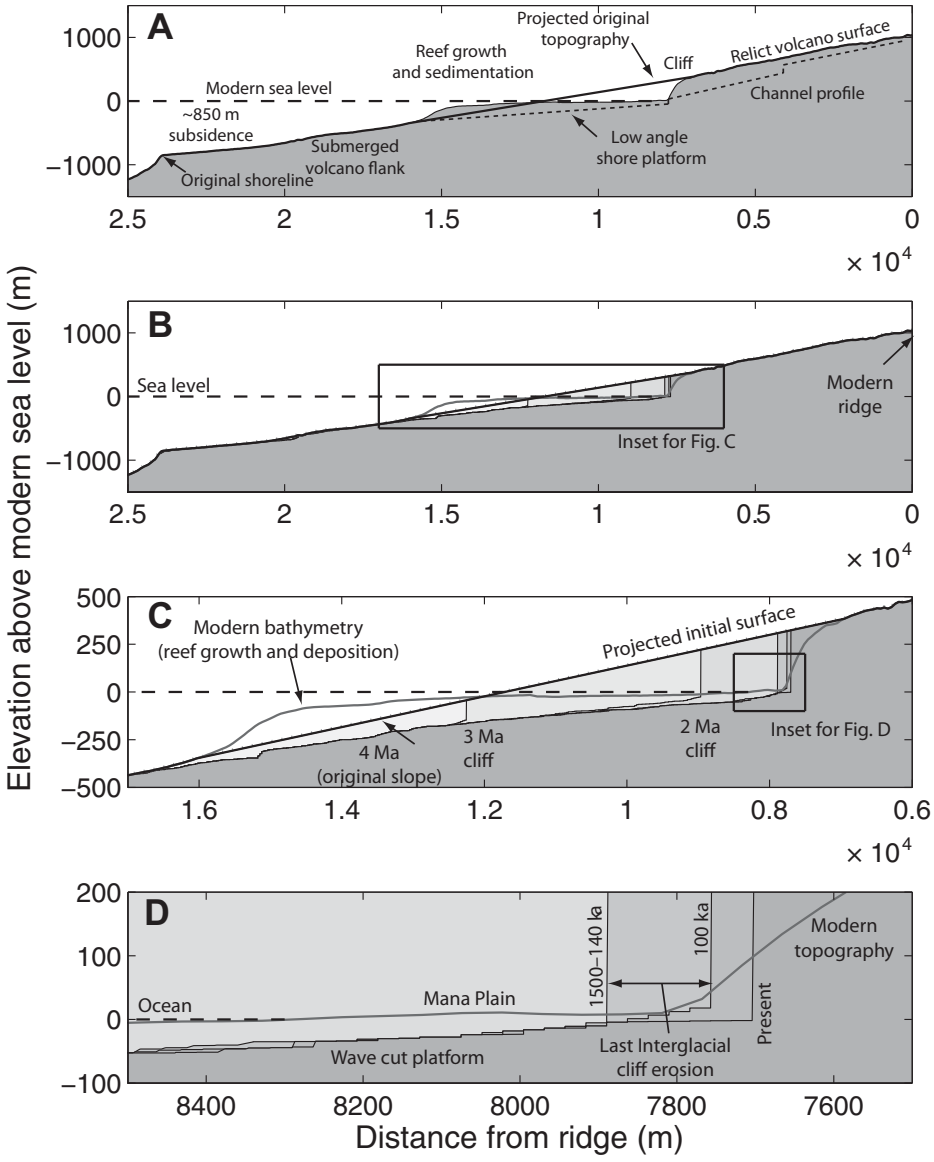

Figure 9. (A) Transect of Kaua'i near Ka'ula'ula Valley heading offshore from the ridge backing onto Waimea Canyon (after Inman et al., 1963). Modern topography from the island transect (Fig. 1) is represented by the gray shading. The pre-eroded volcano profile was reconstructed by projecting offshore the relict volcano surface preserved as interfluves, with deviations from this caused by cliff erosion and offshore sedimentation and coral reef growth. The slope break at 850 m below sea level represents the original island shoreline, which has since subsided. (B) Reconstructed initial island profile used in the cliff retreat model. Superimposed on this profile are the modeled topographic profiles due to cliff erosion. (C) Enlargement of area outlined in black box in B showing model results (solid black lines) of the evolution of the coastal cliff and offshore platform through time. (D) Enlargement at the cliff base from panel C. The cliff did not advance from 1.5 Ma to 130 ka but eroded significantly during the last interglacial.

Kaua'i Sea-Level and Subsidence History

Lithospheric modeling and physical evidence from the Hawai'ian volcanic chain suggest that the volcanoes rapidly subside during and after construction due to loading of the lithosphere (Moore, 1987; Watts and Tenbrink, 1989; Grigg and Jones, 1997). For example, the volcanically active Island of Hawai'i is subsiding at 2.6 mm/yr, based on the ages of drowned Pleistocene coral reefs (Ludwig et al., 1991). The total magnitude of subsidence of northwestern Kaua'i since the end of shield-building volcanism at 4 Ma (Garcia et al., 2010) is well constrained from the drowned slope break ~850 m below sea level. However, due to the loading and flexural response of the ocean crust during construction of adjacent volcanoes, Hawai'ian volcanoes do not have a simple subsidence history. Crustal loading generates proximal moat and distal bulge effects, which can cause uplift, tilting, and subsidence of nearby volcanic islands (Grigg and Jones, 1997). Kaua'i passed over the flexural bulge created during construction of Maui Nui (Maui, Lana'i, Moloka'i, and Kaho'olawe Islands) from 1.5 to 0.5 Ma (Watts and Tenbrink, 1989; Hearty et al., 2005), resulting in marginal uplift. A modern analogue for Kaua'i ca. 1–1.5 Ma is O'ahu, which is being uplifted today at ~0.06 mm/yr as a result of loading due to the Island of Hawai'i (McMurtry et al., 2010). Kaua'i is now beyond the range of lithospheric flexure associated with active volcanism on Hawai'i, and available data based on reef chronology suggest Kaua'i has been largely stable, or slowly subsiding (<0.05 mm/yr), for the past 500 k.y. (Hearty et al., 2005).

To explore the potential effect of changes of sea level driving cliff retreat, we combined approximations of Kaua'i's subsidence history (Grigg and Jones, 1997; Hearty et al., 2005) with the Pleistocene eustatic sea-level record of Miller et al. (2005) (Fig. 11A). Our approach was to assess the intervals during Kaua'i's history when there was potential for waves to erode the primary sea cliff now exposed along the Na Pali coast. Following Inman et al. (1963), we approximated the original island profile by projecting the slope of the interfluves offshore, so that they line up with the distal section of the original volcano surface (Fig. 9A). This analysis shows that over the last ~1.5 m.y., the base of the modern-day coastal cliffs near Ka'ula'ula Valley were only accessible to wave erosion at the last sea-level highstand, ca. 130 ka (Fig. 11A). In the next section, we explore the interplay of sea-level fluctuations, subsidence, and wave erosion in forming the Na Pali coastal cliffs.

Wave Erosion Modeling

To model cliff formation by wave attack, we assumed that erosion occurs at a narrow zone of water depths where waves break. Previous workers have set this zone to be a function of wave height, tidal range, and other processes, and it is typically on the order of meters in thickness (e.g., Ashton et al., 2011). Because we intended to oscillate this breaker zone over hundreds of meters due to sea-level variations and island subsidence, we simply set the erosional zone to be at sea level. Three factors are typically accounted for in the erosion of coasts: beach sediment, which can protect coastal bluffs; the

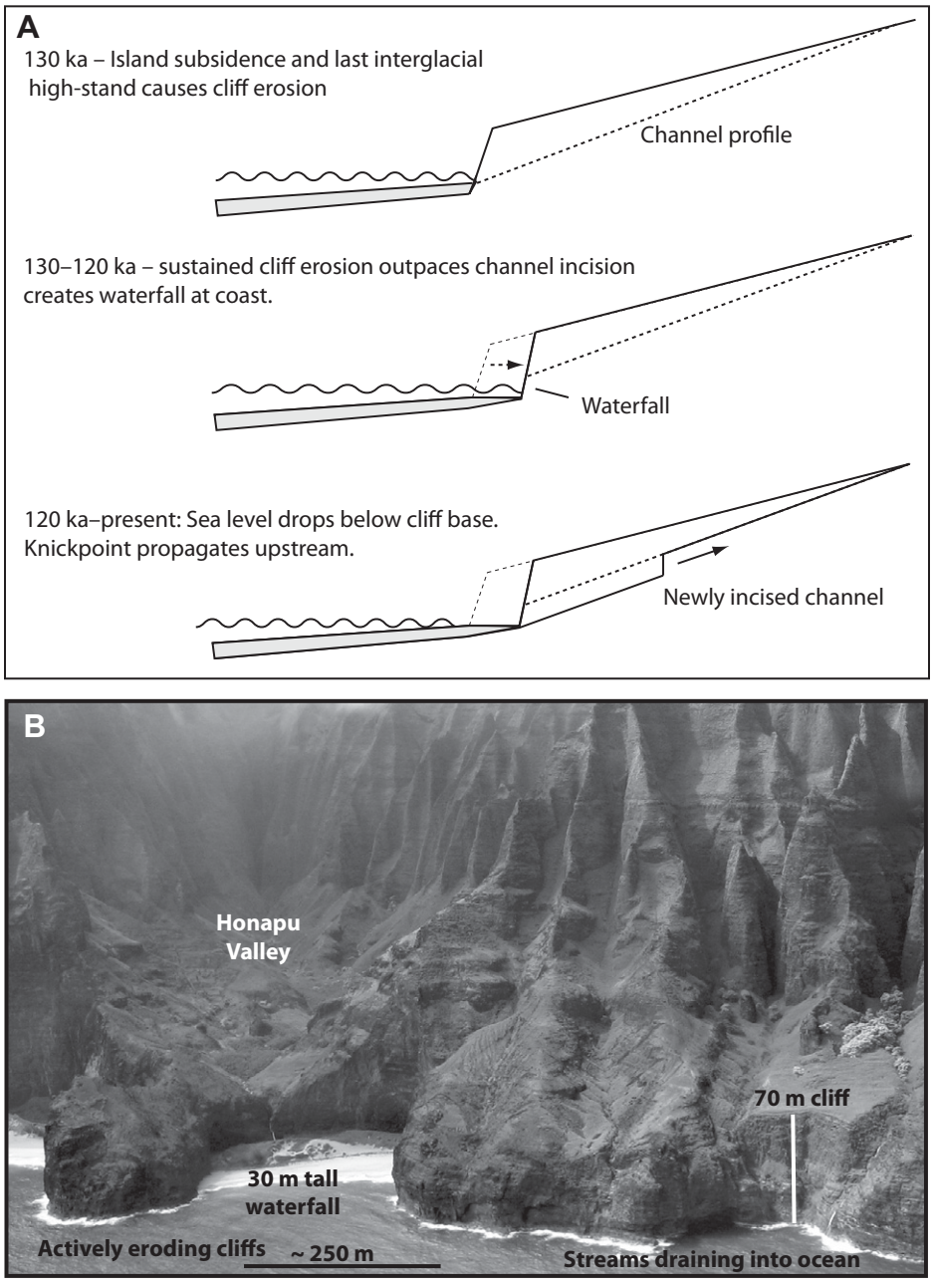

Figure 10. (A) Schematic illustrating our conceptual model for generating coastal cliffs by wave attack and knickpoints for subsiding or stable rocky coasts. Gray shading indicates sediment deposition and reef growth over the shore platform. At sea-level highstand, the shoreline abuts the cliffs, and wave attack causes lateral back wearing. A topographic step is created at the river mouth where the channel profile is steeper than the shoreface and cliff erosion outpaces channel incision. During falling sea level, wave attack shifts away from the primary sea cliff and onto the marine platform, and waterfall erosion causes propagation of the knickpoint upstream. Multiple sea-level cycles may create multiple cycles of local relief generation. (B) Oblique aerial photo of the central Na Pali coast, a possible analogue for the mouth of Ka'ula'ula Valley during the last interglacial (ca. 120 ka). Waves are actively eroding sea cliffs, leaving small streams hanging along the coast. The larger Honapu Valley (~3.3 km^2) has a 35-m-tall waterfall above the 15-m-tall sand dunes. See Figure 1 for location. Image modified from Wikipedia Commons.

slope of the offshore platform, which can dissipate waves; and the slope of the coastal bluff itself, where erosion rates are faster for steeper bluffs due to more energetic wave breaking (e.g., Kamphuis, 1987; Anderson et al., 1999; Ashton et al., 2011; Limber and Murray, 2011). Ashton et al. (2011) suggested that the last effect dominates for rocky coastal cliffs, where collapsed material and beach sediments are easily mobilized. Following this work, and since the Na Pali coastal cliffs are largely slope invariant (i.e., they are subvertical), we simply set the lateral cliff erosion rate to a constant value. Like most hard rocky coastlines, there are no data on the modern rate of cliff retreat along the Na Pali coast, so we varied the cliff retreat rate in our model to find the best-fit value that can explain the location of the modern cliffs.

Starting with the initial reconstructed topographic profile of the volcano (Fig. 9A), and the combined sea level and subsidence record (Fig. 11A), the model uses geometry to determine the location of the shoreline on the volcanic shield at each time step, set to 1 k.y. A notch is cut horizontally into the volcano at a specified erosion rate, and the overburden rock is assumed to be readily removed by wave action (cf. Limber and Murray, 2011). In our model, wave erosion is assumed to occur at a constant rate regardless of whether the shoreline is on the shelf (i.e., cutting a marine platform) or adjacent to the primary sea cliff. Thus, during relative sea-level fall, the sea does not abut the primary sea cliff, so that no erosion of the primary cliff occurs, and instead the shore platform is beveled. In this way, the model readily produces a wide shore platform ~50–100 m beneath modern sea level that conforms with the well-log data beneath the Mana Plain (Macdonald et al., 1960). A constant cliff erosion rate of 27 mm/yr most accurately reproduces the present-day sea-cliff location over the island's 4 m.y. subaerial history.

Our model of cliff erosion for Kaua'i indicates that much of cliff formation occurred early in the island's history, especially in the first 2 m.y. following the end of shield-building volcanism (Figs. 9 and 11B). During this time of persistent subsidence, the sea had frequent access to the primary sea cliff, especially during highstands (Fig. 11B). Some knickpoints generated at sea-level lowstands were subsequently drowned by the combination of sea-level rise and subsidence (e.g., Trenhaile, 2002). The emergence of Kaua'i from 1.5 to 0.5 Ma due to crustal loading by Maui Nui has a major effect on the cliff erosion model, as the modern cliff base was elevated above even the highest sea-level stand over that period (Fig. 11A). Our modeling suggests that for a major portion of the island's history (from 1.5 Ma until ca. 130 ka), the sea did not have

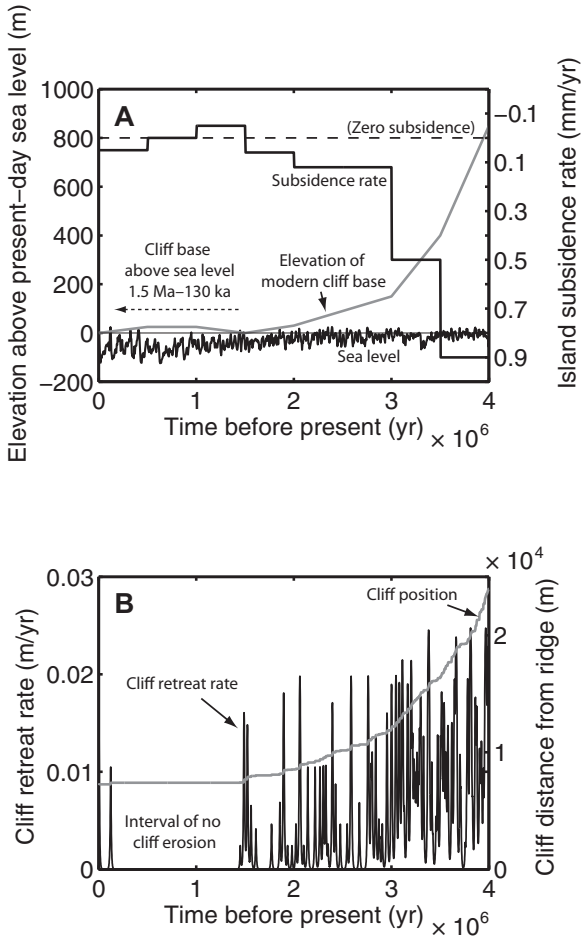

Figure 11. (A) Island subsidence rate, inferred sea-level elevation, and inferred elevation of the base of the modern cliff, relative to present-day sea level. Dashed line indicates zero subsidence. Sea-level reconstruction is from Miller et al. (2005). (B) Modeling results of the primary sea-cliff location through time and cliff retreat rate. All distances are measured from the topographic divide (ridge) at the headwaters of Ka'ula'ula Valley. The annual cliff retreat rate is a constant in the model (i.e., it is either zero or 27 mm/yr), and it appears variable here owing to a low-pass filter with a characteristic time scale of 30 k.y. used to highlight times of substantial cliff erosion at longer time scales.

access to the primary cliff base (Figs. 11A–11B), and the lower reaches of rivers would have extended across a broad, low-sloping coastal plain, where little relief could have been generated at the river mouths via wave erosion. The end of this long hiatus in cliff erosion coincides with the last interglacial at ca. 130 ka, which was a particularly high stand of sea level.

Given our measured vertical incision rates, we consider the hiatus of cliff retreat from 1.5 Ma to 130 ka to be of sufficient duration for the stream channels to have cut through any preexisting sea cliff via knickpoint propagation and vertical incision. Thus, according to the model, the last interglacial period represents the only time in the last 1.5 m.y. that waterfalls at the valley entrance could have been generated via wave erosion. The modeled hiatus in primary cliff erosion from 1.5 Ma to 130 ka, however, is sensitive to the imposed history of subsidence, which is poorly constrained. For example, the model can produce several episodes of cliff cutting during sea level highstand in the last 500 k.y. under different imposed uplift and subsidence histories.

The last interglacial period spanned ca. 130–120 ka (Hearty et al., 2007), an ~10,000 yr period to enable cliff erosion, which, given the model-fit sea-cliff retreat rate of 27 mm/yr, would have produced ~270 m of horizontal cliff retreat. Given the ~13% slope of the modern stream channel, 270 m of wave cutting would have produced a 30–40-m-high escarpment at the river mouth, which is similar to the modern waterfall height of 40 m. An initial waterfall height of 40 m is insufficient to explain the ~200 m of additional valley relief near the river mouth as compared to upstream of the modern waterfall (e.g., Fig. 5), however, which suggests that the downstream part of the valley was steep prior to waterfall generation ca. 120 ka.

Prior to relative sea-level fall at the end of the last interglacial, sea-cliff erosion may have generated hanging streams at the coast, creating waterfalls that discharged directly into the ocean, as illustrated in Figure 10A. Some of the Na Pali coast streams east of the Mana Plain are hanging at their mouths presently (Fig. 10B), suggesting that knickpoint generation is an active process in some locations on the Kaua'i coast where waves cut into steep, canyon-bound channels. We speculate that the base of waterfalls generated at highstands may need to be exposed as sea level falls to allow for knickpoints to retreat inland, as knickpoint retreat must outpace coastal cliff erosion for the knickpoints to propagate inland.

DISCUSSION

Knickpoint Retreat and Debris Flows

Our results suggest that the knickpoint in Ka'ula'ula Valley migrated more rapidly than was reported previously by Seidl et al. (1997), with an average waterfall retreat rate of ~33 mm/yr. This 33 mm/yr rate is faster than many previously documented long-term (>10^6 yr scale) rates of knickpoint retreat (Berlin and Anderson, 2007; Loget and Van Den Driessche, 2009, and references therein); however, it compares well with shorter-term (10^4–10^6 yr) documented retreat rates, including 60 mm/yr for waterfalls in Hawai'ian basaltic rock (Lamb et al., 2007), 10–70 mm/yr in welded ignimbrites (Hayakawa et al., 2008b), 80–150 mm/yr in welded pyroclastic flows (Hayakawa et al., 2008a), and an average of ~15 mm/yr in small drainages in coastal Scotland (Jansen et al., 2011). Our rate is considerably less than knickpoint migration rates of up to 1 m/yr proposed by Crosby and Whipple (2006) in weak marine sedimentary rock, or rates shortly after the Last Glacial Maximum in Scotland (Jansen et al., 2011) attributed to a period of high sediment supply.

One explanation for a small coastal bedrock channel to achieve a relatively fast rate of knickpoint retreat is the nature of the bedrock and the mechanism of erosion. The basalt in Ka'ula'ula Valley is pervasively jointed by bedding planes and cooling joints, which can expedite knickpoint retreat as the jointing enables individual blocks to be plucked from the waterfall face during high flows (Seidl et al., 1996, 1997; Weissel and Seidl, 1998; Lamb et al., 2008; Lamb and Dietrich, 2009). Block toppling at a waterfall face can preferentially preserve the vertical step, which has been shown experimentally by Lamb and Dietrich (2009). Since block plucking and toppling readily occur once a threshold is passed (Lamb and Dietrich, 2009), the ultimate rate of waterfall retreat may be set by the ability of flows to transport sediment away from the waterfall headwall. Despite previous modeling work in Ka'ula'ula Valley that emphasized river incision and fluvial transport processes (Seidl et al., 1994; Chatanantavet and Parker, 2005; Ferrier et al., 2013a), the steep channel gradient and our field observations suggest that downstream of the knickpoint, debris flows, rather than fluvial processes, are likely the rate-limiting step for transport of coarse sediment, and thus may control the rate of waterfall

retreat. This may also explain why the knickpoint retreat rate does not appear to depend on drainage area. Debris flows often initiate at a single location and are advected down channel; thus, a drainage area dependency of debris-flow transport or erosion at the waterfall might not be expected (Stock and Dietrich, 2006).

The channel gradient downstream of the waterfall in Ka'ula'ula Valley is steeper than upstream, and therefore the knickpoint is both a vertical-step knickpoint and a slope-break knickpoint (sensu Haviv et al., 2010). Kirby and Whipple (2012) argued that most vertical-step knickpoints are anchored in space, and that slope-break knickpoints are the primary mechanism for landscape change. In contrast, our study shows that waterfalls can be generated from climate-induced sea-level change, propagate upstream at a rapid rate, and transmit local relief generated at the coast throughout the landscape. Moreover, the steep channel slope downstream of the waterfall in Ka'ula'ula Valley may be a secondary effect related to heightened debris production from the inner gorge and neighboring high-relief hillslopes rather than the primary driver of knickpoint propagation.

If block toppling at the waterfall, rockfall in the inner gorge, and debris-flow transport downstream are the dominant processes in the lower half of Ka'ula'ula Valley, then this can explain why the fine sediment sampled at the mouth of the canyon yields the same accumulation age as the sample taken just upstream of the waterfall lip. If these detrital olivine samples are interpreted as catchment-averaged measurements, then the lower sample should show a younger age, because it should incorporate grains from the rapidly eroding waterfall. However, it is unclear if these samples represent catchment-averaged samples. Unlike measurements of ^{10}Be in more refractory minerals like quartz, for example, olivine readily weathers out of rock. Our observations indicate that hillslope soil and saprolite are largely devoid of olivine on Kaua'i, and thus olivines in sand samples were likely derived from actively eroding areas of the catchment (e.g., in channel; Ferrier et al., 2013b). In addition, sand particles at the river mouth might be undersampling waterfall retreat if the knick zone is shedding boulders, and these boulders are slowly breaking down to sand. This seems likely if the waterfall is eroding by block toppling and plucking, and debris flows are transporting boulders downstream to the boulder fan.

Island Evolution

Our results suggest that channel incision via waterfall retreat may be a primary process by which volcanic islands are dissected once volcanism ceases and subsidence and submergence occur. For volcanic islands, base level is materially driven by a combination of both long-term island subsidence and eustatic fluctuations in sea level. Given the right combination of subsidence, sea-level rise, and offshore topography, cliff erosion can be significant and outpace channel incision, generating knickpoints at river mouths that subsequently propagate upstream. Given eustatic fluctuations in sea level, knickpoint generation on subsiding volcanic islands may be cyclical. For example, the smaller knickpoint in Ka'ula'ula Valley, ~2.5 km upstream from the main waterfall (Fig. 6A), may represent an older episode of sea-cliff cutting and knickpoint formation. If the upper knickpoint is propagating at rates similar to those we measured for the main waterfall, then this would place the upstream knickpoint at the coastal cliffs at ca. 195 ka, coincident with the end of the previous sea-level highstand (stage 7). Although knickpoint formation at ca. 195 ka is inconsistent with our cliff-erosion model predictions, model results are particularly sensitive to the imposed subsidence history (especially when subsidence rates are small), which is only crudely constrained over the past several hundred thousand years (Fig. 11A). Older generations of knickpoints may have propagated through the system entirely. Further support for cycles of knickpoint generation comes from the presence of multiple knickpoints in many of the neighboring Na Pali coast streams (e.g., Seidl et al., 1994; DeYoung, 2000). As shown by our modeling, however, knickpoint formation is not a simple function of sea level and instead depends on the evolving island topography and subsidence rates. Consequently, attempts to explain the range of knickpoints using river-profile analysis in the Na Pali coast streams without multiple (and in cases localized) changes in base level have had limited success (DeYoung, 2000).

Our data indicate that the average rate of knickpoint retreat (33 mm/yr) is three orders of magnitude greater than long-term rates of vertical incision and putative catchment-averaged rates (0.027 mm/yr) derived from cosmogenic ^{3}He exposure data. This emphasizes the role that knickpoint propagation can have in generating valley relief. The passage of the 40-m-high waterfall has generated up to 40% of the relief in the middle parts of Ka'ula'ula Valley, in 3% of the time since the volcanic topography was formed. The measured waterfall retreat rates from Ka'ula'ula Valley are so great that they likely dominate the sediment flux from the valley. For example, a vertical incision rate of 0.022 mm/yr applied over the entire length of the valley (10 km) results in a sediment yield per unit channel width of 0.22 m^2/yr. Considering a waterfall retreat rate of 33 mm/yr and a waterfall height of 40 m, we find a sediment yield per unit channel width for the waterfall alone of 1.2 m^2/yr, roughly fivefold the apparent yield from vertical incision.

Recognition that island erosion rates and local sediment yields can fluctuate significantly on 10–100 k.y. time scales has significant implications for island sediment budgets and erosion-rate studies. For example, there is a major effort to place modern sediment fluxes on the Hawai'ian Islands in the context of long-term rates given concerns with the sustainability of coral reef habitat (Ogston et al., 2004; Stock and Tribble, 2010). Our study suggests that estimating long-term sediment yield over the age of the volcano by differencing reconstructed volcano surfaces from the modern topography may significantly underestimate sediment yield over the last tens of thousands of years where knickpoints are active. The possibility of sea-level–driven cycles of erosion suggests that recently proposed precipitation rate–dependent erosion laws developed for million-year time scales (Ferrier et al., 2013a) may not be applicable to the shorter (10^2–10^5 yr) time scales over which we observe knickpoints to propagate in this environment. In addition, measurements of cosmogenic exposure ages from sand samples at the mouth of catchments, a common technique for constraining catchment-averaged erosion rates (e.g., Bierman and Steig, 1996; Granger et al., 1996; Ferrier et al., 2013b), may underrepresent the erosion contribution of propagating waterfalls if knickpoints erode by block failure rather than grain-scale abrasion, in a manner similar to catchments prone to deep-seated landsliding (e.g., Yanites et al., 2009).

CONCLUSION

We used cosmogenic ^{3}He exposure dating to constrain the rate of knickpoint retreat in Ka'ula'ula Valley, Kaua'i, Hawai'i. Our ^{3}He measurements are consistent with knickpoint initiation at ca. 120 ka, leading to waterfall migration nearly 4 km up the valley at a constant rate of 33 mm/yr, i.e., far faster than previous estimates. The fractured nature of the basalt may facilitate both rapid knickpoint retreat rate by block plucking, and the maintenance of the vertical waterfall face. Passage of the knickpoint had a major effect on valley morphology, leaving steep cliffs, boulder-strewn terraces, and a persistently steep channel (13%), in comparison to the soil-mantled landscape upstream. Field observations and topographic analysis indicate that debris flows are prevalent and likely represent the dominant transport mechanism downstream of the waterfall. Sea-level and

subsidence histories point to the last interglacial (ca. 130–120 ka) as the time when waves were able to cut into the steep, canyon-bound channel bed at the river mouth, leading to the initiation of a waterfall. Cliff erosion and subsequent knickpoint retreat may be important relief-generating mechanisms that drive erosion in other landscapes with stable or subsiding coasts where stream gradients exceed shore-platform slopes.

ACKNOWLEDGMENTS

This study was funded by the National Science Foundation (NSF) grants EAR-1204375 and EAR-1147381 to Lamb. Light detection and ranging (LiDAR) data were collected by the NSF National Center for Airborne Laser Mapping with a seed grant to Mathieu Lapotre. We thank Will Amidon and Lindsey Hedges for help in processing the cosmogenic ^{3}He samples. We had discussions with and field support from Taylor Perron, Ken Ferrier, Sujoy Mukhopadhyay, Matt Rosener, and Chuck Blay. Thorough reviews from Ken Ferrier, Kelin Whipple, Joel Johnson, an anonymous reviewer, and *GSA Bulletin* associate editor Anne Jefferson greatly improved this manuscript.

REFERENCES CITED

Abbuhl, L.M., Norton, K.P., Jansen, J.D., Schlunegger, F., Aldahan, A., and Possnert, G., 2011, Erosion rates and mechanisms of knickzone retreat inferred from ^{10}Be measured across strong climate gradients on the northern and central Andes Western Escarpment: Earth Surface Processes and Landforms, v. 36, p. 1464–1473, doi:10.1002/esp.2164.

Aldrich, L.T., and Nier, A.O., 1948, The occurrence of He^3 in natural sources of helium: Physical Review, v. 74, p. 1590–1594, doi:10.1103/PhysRev.74.1590.

Amidon, W.H., and Farley, K.A., 2011, Cosmogenic He-3 production rates in apatite, zircon and pyroxene inferred from Bonneville flood erosional surfaces: Quaternary Geochronology, v. 6, p. 10–21, doi:10.1016/j.quageo.2010.03.005.

Amidon, W.H., Rood, D.H., and Farley, K.A., 2009, Cosmogenic He-3 and Ne-21 production rates calibrated against Be-10 in minerals from the Coso volcanic field: Earth and Planetary Science Letters, v. 280, p. 194–204, doi:10.1016/j.epsl.2009.01.031.

Anderson, R.S., Densmore, A.L., and Ellis, M.A., 1999, The generation and degradation of marine terraces: Basin Research, v. 11, p. 7–19, doi:10.1046/j.1365-2117.1999.00085.x.

Andrews, J.N., and Kay, R.L.F., 1982, Natural production of tritium in permeable rocks: Nature, v. 298, p. 361–363, doi:10.1038/298361a0.

Ashton, A.D., Walkden, M.J.A., and Dickson, M.E., 2011, Equilibrium responses of cliffed coasts to changes in the rate of sea level rise: Marine Geology, v. 284, p. 217–229, doi:10.1016/j.margeo.2011.01.007.

Balco, G., Stone, J.O., Lifton, N.A., and Dunai, T.J., 2008, A complete and easily accessible means of calculating surface exposure ages or erosion rates from Be-10 and Al-26 measurements: Quaternary Geochronology, v. 3, p. 174–195, doi:10.1016/j.quageo.2007.12.001.

Berlin, M.M., and Anderson, R.S., 2007, Modeling of knickpoint retreat on the Roan Plateau, western Colorado: Journal of Geophysical Research–Earth Surface, v. 112, F03S06, doi:10.1029/2006JF000553.

Bierman, P., and Steig, E.J., 1996, Estimating rates of denudation using cosmogenic isotope abundances in sediment: Earth Surface Processes and Landforms, v. 21, p. 125–139, doi:10.1002/(SICI)1096-9837(199602)21:2<125::AID-ESP511>3.0.CO;2-8.

Bishop, P., Hoey, T.B., Jansen, J.D., and Artza, I.L., 2005, Knickpoint recession rate and catchment area: The case of uplifted rivers in eastern Scotland: Earth Surface Processes and Landforms, v. 30, p. 767–778, doi:10.1002/esp.1191.

Blard, P.H., and Farley, K.A., 2008, The influence of radiogenic He-4 on cosmogenic He-3 determinations in volcanic olivine and pyroxene: Earth and Planetary Science Letters, v. 276, p. 20–29, doi:10.1016/j.epsl.2008.09.003.

Cerling, T.E., and Craig, H., 1994, Geomorphology and in-situ cosmogenic isotopes: Annual Review of Earth and Planetary Sciences, v. 22, p. 273–317, doi:10.1146/annurev.ea.22.050194.001421.

Chatanantavet, P., and Parker, G., 2005, Modeling the bedrock river evolution of western Kaua'i, Hawai'i, by a physically-based incision model based on abrasion, *in* Parker, G., and Garcia, M.H., eds., River, Coastal and Estuarine Morphodynamics: London, Taylor and Francis, p. 99–101.

Clague, D.A., and Dalrymple, G.B., 1988, Age and petrology of alkalic postshield and rejuvenated-stage lava from Kauai, Hawaii: Contributions to Mineralogy and Petrology, v. 99, p. 202–218, doi:10.1007/BF00371461.

Cook, K.L., Turowski, J.M., and Hovius, N., 2013, A demonstration of the importance of bedload transport for fluvial bedrock erosion and knickpoint propagation: Earth Surface Processes and Landforms, v. 38, p. 683–695, doi:10.1002/esp.3313.

Craig, H., and Poreda, R.J., 1986, Cosmogenic ^{3}He in terrestrial rocks: The summit lavas of Maui: Proceedings of the National Academy of Sciences of the United States of America, v. 83, p. 1970–1974, doi:10.1073/pnas.83.7.1970.

Crosby, B.T., and Whipple, K.X., 2006, Knickpoint initiation and distribution within fluvial networks: 236 waterfalls in the Waipaoa River, North Island, New Zealand: Geomorphology, v. 82, p. 16–38, doi:10.1016/j.geomorph.2005.08.023.

DeYoung, V.N., 2000, Modeling the Geomorphic Evolution of Western Kauai, Hawaii; A Study of Surface Processes in a Basaltic Terrain: Halifax, Nova Scotia, Canada, Dalhousie University, 165 p.

DiBiase, R.A., Whipple, K.X., Heimsath, A.M., and Ouimet, W.B., 2010, Landscape form and millennial erosion rates in the San Gabriel Mountains, CA: Earth and Planetary Science Letters, v. 289, p. 134–144, doi:10.1016/j.epsl.2009.10.036.

Dorsey, R.J., and Roering, J.J., 2006, Quaternary landscape evolution in the San Jacinto fault zone, Peninsular Ranges of Southern California: Transient response to strike-slip fault initiation: Geomorphology, v. 73, p. 16–32, doi:10.1016/j.geomorph.2005.06.013.

Dunai, T.J., and Wijbrans, J.R., 2000, Long-term cosmogenic ^{3}He production rates (152 ka–1.35 Ma) from ^{40}Ar/^{39}Ar dated basalt flows at 29°N latitude: Earth and Planetary Science Letters, v. 176, p. 147–156, doi:10.1016/S0012-821X(99)00308-8.

Fenton, C.R., Niedermann, S., Goethals, M.M., Schneider, B., and Wijbrans, J., 2009, Evaluation of cosmogenic He-3 and Ne-21 production rates in olivine and pyroxene from two Pleistocene basalt flows, western Grand Canyon, AZ, USA: Quaternary Geochronology, v. 4, p. 475–492, doi:10.1016/j.quageo.2009.08.002.

Ferrier, K.L., Huppert, K.L., and Perron, J.T., 2013a, Climatic control of bedrock river incision: Nature, v. 496, p. 206–209, doi:10.1038/nature11982.

Ferrier, K.L., Perron, J.T., Mukhopadhyay, S., Rosener, M., Stock, J.D., Huppert, K.L., and Slosberg, M., 2013b, Covariation of climate and long-term erosion rates across a steep rainfall gradient on the Hawaiian island of Kaua'i: Geological Society of America Bulletin, v. 125, p. 1146–1163, doi:10.1130/B30726.1.

Flinders, A.F., Ito, G., and Garcia, M.O., 2010, Gravity anomalies of the Northern Hawaiian Islands: Implications on the shield evolutions of Kauai and Niihau: Journal of Geophysical Research–Solid Earth, v. 115, B08412, doi:10.1029/2009JB006877.

Fuller, T.K., Perg, L.A., Willenbring, J.K., and Lepper, K., 2009, Field evidence for climate-driven changes in sediment supply leading to strath terrace formation: Geology, v. 37, p. 467–470, doi:10.1130/G25487A.1.

Gallen, S.F., Wegmann, K.W., Frankel, K.L., Hughes, S., Lewis, R.Q., Lyons, N., Paris, P., Ross, K., Bauer, J.B., and Witt, A.C., 2011, Hillslope response to knickpoint migration in the Southern Appalachians: Implications for the evolution of post-orogenic landscapes: Earth Surface Processes and Landforms, v. 36, p. 1254–1267, doi:10.1002/esp.2150.

Garcia, M.O., Swinnard, L., Weis, D., Greene, A.R., Tagami, T., Sano, H., and Gandy, C.E., 2010, Petrology, geochemistry and geochronology of Kaua'i lavas over 4.5 Myr: Implications for the origin of rejuvenated volcanism and the evolution of the Hawaiian plume: Journal of Petrology, v. 51, p. 1507–1540, doi:10.1093/petrology/egq027.

Gayer, E., Mukhopadhyay, S., and Meade, B.J., 2008, Spatial variability of erosion rates inferred from the frequency distribution of cosmogenic He-3 in olivines from Hawaiian river sediments: Earth and Planetary Science Letters, v. 266, p. 303–315, doi:10.1016/j.epsl.2007.11.019.

Gilbert, G.K., 1890, The History of the Niagara River, Extracted from The Sixth Annual Report of the Commissioners of the State Reservation at Niagara, for the Year 1889: Albany, New York, J.B. Lyon, printer, 84 p.

Gillen, D., Honda, M., Chivas, A.R., Yatsevich, I., Patterson, D.B., and Carr, P.F., 2010, Cosmogenic ^{21}Ne exposure dating of young basaltic lava flows from the Newer Volcanic Province, western Victoria, Australia: Quaternary Geochronology, v. 5, p. 1–9, doi:10.1016/j.quageo.2009.08.004.

Goehring, B.M., Kurz, M.D., Balco, G., Schaefer, J.M., Licciardi, J., and Lifton, N., 2010, A reevaluation of in situ cosmogenic He-3 production rates: Quaternary Geochronology, v. 5, p. 410–418, doi:10.1016/j.quageo.2010.03.001.

Gosse, J.C., and Phillips, F.M., 2001, Terrestrial in situ cosmogenic nuclides: Theory and application: Quaternary Science Reviews, v. 20, p. 1475–1560, doi:10.1016/S0277-3791(00)00171-2.

Granger, D.E., Kirchner, J.W., and Finkel, R., 1996, Spatially averaged long-term erosion rates measured from in situ–produced cosmogenic nuclides in alluvial sediment: The Journal of Geology, v. 104, p. 249–257, doi:10.1086/629823.

Grigg, R.W., and Jones, A.T., 1997, Uplift caused by lithospheric flexure in the Hawaiian Archipelago as revealed by elevated coral deposits: Marine Geology, v. 141, p. 11–25, doi:10.1016/S0025-3227(97)00069-8.

Hanks, T.C., 2000, The age of scarplike landforms from diffusion-equation analysis, *in* Noller, J.S., Sowers, J.M., and Lettis, W.R. eds., Quaternary Geochronology: Methods and Applications, Volume 4: American Geophysical Union Reference Shelf: Washington, DC, American Geophysical Union, p. 313–338.

Haviv, I., Enzel, Y., Whipple, K.X., Zilberman, E., Matmon, A., Stone, J., and Fifield, K.L., 2010, Evolution of vertical knickpoints (waterfalls) with resistant caprock: Insights from numerical modeling: Journal of Geophysical Research–Earth Surface, v. 115, F03028, doi:10.1029/2008JF001187.

Hayakawa, Y.S., Obanawa, H., and Matsukura, Y., 2008a, Post-volcanic erosion rates of Shomyo Falls in Tateyama, central Japan: Geografiska Annaler, ser. A, Physical Geography, v. 90A, p. 65–74.

Hayakawa, Y.S., Yokoyama, S., and Matsukura, Y., 2008b, Erosion rates of waterfalls in post-volcanic fluvial systems around Aso volcano, southwestern Japan: Earth Surface Processes and Landforms, v. 33, p. 801–812, doi:10.1002/esp.1615.

Hearty, P.J., Kaufman, D.S., Olson, S.L., and James, H.F., 2000, Stratigraphy and whole-rock amino acid geochronology of key Holocene and last interglacial carbonate deposits in the Hawaiian Islands: Pacific Science, v. 54, p. 423–442.

Hearty, P.J., Karner, D.B., Renne, P.R., Olson, S.L., and Fletcher, S., 2005, (40)Ar/(39)Ar age of a young rejuvenation basalt flow: Implications for the duration of volcanism and the timing of carbonate platform development during the Quaternary on Kaua'i, Hawaiian Islands: New Zealand Journal of Geology and Geophysics, v. 48, p. 199–211, doi:10.1080/00288306.2005.9515110.

Hearty, P.J., Hollin, J.T., Neumann, A.C., O'Leary, M.J., and McCulloch, M., 2007, Global sea-level fluctuations during the last interglaciation (MIS 5e): Quaternary

Science Reviews, v. 26, p. 2090–2112, doi:10.1016/j.quascirev.2007.06.019.

Hinds, N.E.A., 1925, Amphitheater valley heads: The Journal of Geology, v. 33, p. 816–818, doi:10.1086/623262.

Hinds, N.E.A., 1930, The Geology of Kauai and Niihau: Honolulu, Hawaii, Bernice P. Bishop Museum, 103 p.

Howard, A.D., Dietrich, W.E., and Seidl, M.A., 1994, Modeling fluvial erosion on regional to continental scales: Journal of Geophysical Research–Solid Earth, v. 99, p. 13,971–13,986, doi:10.1029/94JB00744.

Inman, D.L., Gayman, W.R., and Cox, D.C., 1963, Littoral sedimentary processes on Kauai, a subtropical high island: Pacific Science, v. 17, p. 106–130.

Jakica, S., Quigley, M.C., Sandiford, M., Clark, D., Fifield, L.K., and Alimanovic, A., 2011, Geomorphic and cosmogenic nuclide constraints on escarpment evolution in an intraplate setting, Darling Escarpment, Western Australia: Earth Surface Processes and Landforms, v. 36, p. 449–459, doi:10.1002/esp.2058.

Jansen, J.D., Fabel, D., Bishop, P., Xu, S., Schnabel, C., and Codilean, A.T., 2011, Does decreasing paraglacial sediment supply slow knickpoint retreat?: Geology, v. 39, p. 543–546, doi:10.1130/G32018.1.

Jefferson, A., Grant, G.E., Lewis, S.L., and Lancaster, S.T., 2010, Coevolution of hydrology and topography on a basalt landscape in the Oregon Cascade Range, USA: Earth Surface Processes and Landforms, v. 35, p. 803–816.

Kamphuis, J.W., 1987, Recession rate of glacial till bluffs: Journal of Waterway, Port, Coastal, and Ocean Engineering, v. 113, p. 60–73, doi:10.1061/(ASCE)0733-950X(1987)113:1(60).

Kirby, E., and Whipple, K.X., 2012, Expression of active tectonics in erosional landscapes: Journal of Structural Geology, v. 44, p. 54–75, doi:10.1016/j.jsg.2012.07.009.

Kochel, R.C., and Piper, J.F., 1986, Morphology of large valleys on Hawaii: Evidence for groundwater sapping and comparisons with Martian valleys: Journal of Geophysical Research–Solid Earth, v. 91, p. E175–E192, doi:10.1029/JB091iB13p0E175.

Korup, O., and Schlunegger, F., 2007, Bedrock landsliding, river incision, and transience of geomorphic hillslope-channel coupling: Evidence from inner gorges in the Swiss Alps: Journal of Geophysical Research–Earth Surface, v. 112, F03027, doi:10.1029/2006JF000710.

Kurz, M.D., 1986, In situ production of terrestrial cosmogenic helium and some applications to geochronology: Geochimica et Cosmochimica Acta, v. 50, p. 2855–2862, doi:10.1016/0016-7037(86)90232-2.

Lal, D., 1987, Production of He-3 in terrestrial rocks: Chemical Geology, v. 66, p. 89–98.

Lal, D., 1991, Cosmic-ray labeling of erosion surfaces—In situ nuclide production-rates and erosion models: Earth and Planetary Science Letters, v. 104, p. 424–439, doi:10.1016/0012-821X(91)90220-C.

Lamb, M.P., and Dietrich, W.E., 2009, The persistence of waterfalls in fractured rock: Geological Society of America Bulletin, v. 121, p. 1123–1134, doi:10.1130/B26482.1.

Lamb, M.P., Howard, A.D., Johnson, J., Whipple, K.X., Dietrich, W.E., and Perron, J.T., 2006, Can springs cut canyons into rock?: Journal of Geophysical Research. Planets, v. 111, E07002, doi:10.1029/2005JE002663.

Lamb, M.P., Howard, A.D., Dietrich, W.E., and Perron, J.T., 2007, Formation of amphitheater-headed valleys by waterfall erosion after large-scale slumping on Hawai'i: Geological Society of America Bulletin, v. 119, p. 805–822, doi:10.1130/B25986.1.

Lamb, M.P., Dietrich, W.E., Aciego, S.M., DePaolo, D.J., and Manga, M., 2008, Formation of Box Canyon, Idaho, by megaflood: Implications for seepage erosion on Earth and Mars: Science, v. 320, p. 1067–1070, doi:10.1126/science.1156630.

Leckie, D.A., 1994, Canterbury Plains, New Zealand—Implications for sequence stratigraphic models: American Association of Petroleum Geologists Bulletin, v. 78, p. 1240–1256.

Leyland, J., and Darby, S.E., 2008, An empirical-conceptual gully evolution model for channelled sea cliffs: Geomorphology, v. 102, p. 419–434, doi:10.1016/j.geomorph.2008.04.017.

Leyland, J., and Darby, S.E., 2009, Effects of Holocene climate and sea-level changes on coastal gully evolution: Insights from numerical modelling: Earth Surface Processes and Landforms, v. 34, p. 1878–1893, doi:10.1002/esp.1872.

Licciardi, J.M., Kurz, M.D., Clark, P.U., and Brook, E.J., 1999, Calibration of cosmogenic He-3 production rates from Holocene lava flows in Oregon, USA, and effects of the Earth's magnetic field: Earth and Planetary Science Letters, v. 172, p. 261–271, doi:10.1016/S0012-821X(99)00204-6.

Lifton, N.A., Jull, A.J.T., and Quade, J., 2001, A new extraction technique and production rate estimate for in situ cosmogenic ^{14}C in quartz: Geochimica et Cosmochimica Acta, v. 65, p. 1953–1969, doi:10.1016/S0016-7037(01)00566-X.

Limber, P.W., and Murray, A.B., 2011, Beach and sea-cliff dynamics as a driver of long-term rocky coastline evolution and stability: Geology, v. 39, p. 1147–1150, doi:10.1130/G32315.1.

Loget, N., and Van Den Driessche, J., 2009, Wave train model for knickpoint migration: Geomorphology, v. 106, p. 376–382, doi:10.1016/j.geomorph.2008.10.017.

Ludwig, K.R., Szabo, B.J., Moore, J.G., and Simmons, K.R., 1991, Crustal subsidence rate off Hawaii determined from U-234/U-238 ages of drowned coral reefs: Geology, v. 19, p. 171–174, doi:10.1130/0091-7613(1991)019<0171:CSROHD>2.3.CO;2.

Maaloe, S., James, D., Smedley, P., Petersen, S., and Garmann, L.B., 1992, The Koloa Volcanic Suite of Kauai, Hawaii: Journal of Petrology, v. 33, p. 761–784, doi:10.1093/petrology/33.4.761.

Macdonald, G.A., Davis, D.A., and Cox, D.C., 1960, Geology and Ground-Water Resources of the Island of Kauai, Hawaii: Hawaii Division of Hydrography Bulletin 13, 212 p.

Mackey, B.H., and Lamb, M.P., 2013, Deciphering boulder mobility and erosion from cosmogenic nuclide exposure dating: Journal of Geophysical Research–Earth Surface, v. 118, p. 184–197, doi:10.1002/jgrf.20035.

Margerison, H.R., Phillips, W.M., Stuart, F.M., and Sugden, D.E., 2005, Cosmogenic ^{3}He concentrations in ancient flood deposits from the Coombs Hills, northern Dry Valleys, East Antarctica: Interpreting exposure ages and erosion rates: Earth and Planetary Science Letters, v. 230, p. 163–175, doi:10.1016/j.epsl.2004.11.007.

Mark, R.K., and Moore, J.G., 1987, Slopes of the Hawaiian Ridge, *in* Decker, R.W., Wright, T.L., and Stauffer, P.H., eds., Volcanism in Hawaii: U.S. Geological Survey Professional Paper 1350, p. 101–107.

McDougall, I., 1979, Age of shield-building volcanism of Kauai and linear migration of volcanism in the Hawaiian island chain: Earth and Planetary Science Letters, v. 46, p. 31–42, doi:10.1016/0012-821X(79)90063-3.

McKean, J.A., Dietrich, W.E., Finkel, R.C., Southon, J.R., and Caffee, M.W., 1993, Quantification of soil production and downslope creep rates from cosmogenic Be-10 accumulations on a hillslope profile: Geology, v. 21, p. 343–346, doi:10.1130/0091-7613(1993)021<0343:QOSPAD>2.3.CO;2.

McMurtry, G.M., Watts, P., Fryer, G.J., Smith, J.R., and Imamura, F., 2004, Giant landslides, mega-tsunamis, and paleo–sea level in the Hawaiian Islands: Marine Geology, v. 203, p. 219–233, doi:10.1016/S0025-3227(03)00306-2.

McMurtry, G.M., Campbell, J.F., Fryer, G.J., and Fietzke, J., 2010, Uplift of Oahu, Hawaii, during the past 500 k.y. as recorded by elevated reef deposits: Geology, v. 38, p. 27–30, doi:10.1130/G30378.1.

Menking, J.A., Han, J., Gasparini, N.M., and Johnson, J.P.L., 2013, The effects of precipitation gradients on river profile evolution on the Big Island of Hawai'i: Geological Society of America Bulletin, v. 125, p. 594–608, doi:10.1130/B30625.1.

Miller, K.G., Kominz, M.A., Browning, J.V., Wright, J.D., Mountain, G.S., Katz, M.E., Sugarman, P.J., Cramer, B.S., Christie-Blick, N., and Pekar, S.F., 2005, The Phanerozoic record of global sea-level change: Science, v. 310, p. 1293–1298, doi:10.1126/science.1116412.

Moore, J.G., 1987, Subsidence of the Hawaiian Ridge, *in* Decker, R.W., Wright, T.L., and Stauffer, P.H., eds., Volcanism in Hawaii: U.S. Geological Survey Professional Paper 1350, p. 85–100.

Moore, J.G., Clague, D.A., Holcomb, R.T., Lipman, P.W., Normark, W.R., and Torresan, M.E., 1989, Prodigious submarine landslides on the Hawaiian Ridge: Journal of Geophysical Research–Solid Earth and Planets, v. 94, p. 17,465–17,484, doi:10.1029/JB094iB12p17465.

Moore, J.G., Normark, W.R., and Holcomb, R.T., 1994, Giant Hawaiian landslides: Annual Review of Earth and Planetary Sciences, v. 22, p. 119–144, doi:10.1146/annurev.ea.22.050194.001003.

Morrison, P., and Pine, J., 1955, Radiogenic origin of the helium isotopes in rock: Annals of the New York Academy of Sciences, v. 62, p. 71–92, doi:10.1111/j.1749-6632.1955.tb35366.x.

Mukhopadhyay, S., Lassiter, J.C., Farley, K.A., and Bogue, S.W., 2003, Geochemistry of Kauai shield-stage lavas: Implications for the chemical evolution of the Hawaiian plume: Geochemistry Geophysics Geosystems, v. 4, doi:10.1029/2002GC000342.

Niedermann, S., 2002, Cosmic-ray–produced noble gases in terrestrial rocks: Dating tools for surface processes, *in* Porcelli, D., Ballentine, C.J., and Wieler, R., eds., Noble Gases in Geochemistry and Cosmochemistry: Mineralogical Society of America Reviews in Mineralogy and Geochemistry, v. 47, p. 731–784.

Ogston, A.S., Storlazzi, C.D., Field, M.E., and Presto, M.K., 2004, Sediment resuspension and transport patterns on a fringing reef flat, Molokai, Hawaii: Coral Reefs, v. 23, p. 559–569.

Ramalho, R.S., Quartau, R., Trenhaile, A.S., Mitchell, N.C., Woodroffe, C.D., and Ávila, S.P., 2013, Coastal evolution on volcanic oceanic islands: A complex interplay between volcanism, erosion, sedimentation, sea-level change and biogenic production: Earth-Science Reviews, v. 127, p. 140–170.

Reinhardt, L.J., Bishop, P., Hoey, T.B., Dempster, T.J., and Sanderson, D.C.W., 2007, Quantification of the transient response to base-level fall in a small mountain catchment: Sierra Nevada, southern Spain: Journal of Geophysical Research–Earth Surface, v. 112, F03S05, doi:10.1029/2006JF000524.

Reusser, L.J., Bierman, P.R., Pavich, M.J., Zen, E.A., Larsen, J., and Finkel, R., 2004, Rapid late Pleistocene incision of Atlantic passive-margin river gorges: Science, v. 305, p. 499–502, doi:10.1126/science.1097780.

Righter, K., Caffee, M., Rosas-Elguera, J., and Valencia, V., 2010, Channel incision in the Rio Atenguillo, Jalisco, Mexico, defined by (36)Cl measurements of bedrock: Geomorphology, v. 120, p. 279–292, doi:10.1016/j.geomorph.2010.04.001.

Roering, J.J., Kirchner, J.W., and Dietrich, W.E., 1999, Evidence for nonlinear, diffusive sediment transport on hillslopes and implications for landscape morphology: Water Resources Research, v. 35, p. 853–870, doi:10.1029/1998WR900090.

Rosenbloom, N.A., and Anderson, R.S., 1994, Hillslope and channel evolution in a marine terraced landscape, Santa-Cruz, California: Journal of Geophysical Research–Solid Earth, v. 99, p. 14,013–14,029, doi:10.1029/94JB00048.

Schopka, H.H., and Derry, L.A., 2012, Chemical weathering fluxes from volcanic islands and the importance of groundwater: The Hawaiian example: Earth and Planetary Science Letters, v. 339–340, p. 67–78, doi:10.1016/j.epsl.2012.05.028.

Seidl, M.A., 1993, Form and Process in Channel Incision of Bedrock: Berkeley, California, University of California at Berkeley, 452 p.

Seidl, M.A., Dietrich, W.E., and Kirchner, J.W., 1994, Longitudinal profile development into bedrock—An analysis of Hawaiian channels: The Journal of Geology, v. 102, p. 457–474, doi:10.1086/629686.

Seidl, M.A., Weissel, J.K., and Pratson, L.F., 1996, The kinematics and pattern of escarpment retreat across the rifted continental margin of SE Australia: Basin Research, v. 8, p. 301–316, doi:10.1046/j.1365-2117.1996.00266.x.

Seidl, M.A., Finkel, R.C., Caffee, M.W., Hudson, G.B., and Dietrich, W.E., 1997, Cosmogenic isotope analyses applied to river longitudinal profile evolution: Problems and interpretations: Earth Surface Processes and Landforms, v. 22, p. 195–209, doi:10.1002/(SICI)1096-9837(199703)22:3<195::AID-ESP748>3.0.CO;2-0.

Sherrod, D.R., Sinton, J.M., Watkins, S.E., and Brunt, K.M., 2007, Geologic Map of the State of Hawai'i: U.S. Geological Survey Open-File Report 2007-1089, 83 p.

Snyder, N.P., 2009, Studying stream morphology with airborne laser elevation data: Eos, Transactions, American Geophysical Union, v. 90, p. 45–46, doi:10.1029/2009EO060001.

Snyder, N.P., Whipple, K.X., Tucker, G.E., and Merritts, D.J., 2000, Landscape response to tectonic forcing: Digital elevation model analysis of stream profiles in the Mendocino triple junction region, northern California: Geological Society of America Bulletin, v. 112, p. 1250–1263, doi:10.1130/0016-7606(2000)112<1250:LRTTFD>2.0.CO;2.

Snyder, N.P., Whipple, K.X., Tucker, G.E., and Merritts, D.J., 2002, Interactions between onshore bedrock-channel incision and nearshore wave-base erosion forced by eustasy and tectonics: Basin Research, v. 14, p. 105–127, doi:10.1046/j.1365-2117.2002.00169.x.

Stearns, H.T., 1985, Geology of the State of Hawaii: Palo Alto, California, Pacific Books, 266 p.

Stock, J., and Dietrich, W.E., 2003, Valley incision by debris flows: Evidence of a topographic signature: Water Resources Research, v. 39, 1089, doi:10.1029/2001WR001057.

Stock, J.D., and Dietrich, W.E., 2006, Erosion of steepland valleys by debris flows: Geological Society of America Bulletin, v. 118, p. 1125–1148, doi:10.1130/B25902.1.

Stock, J.D., and Montgomery, D.R., 1999, Geologic constraints on bedrock river incision using the stream power law: Journal of Geophysical Research–Solid Earth, v. 104, p. 4983–4993, doi:10.1029/98JB02139.

Stock, J.D., and Tribble, G., 2010, Erosion and sediment load from two Hawaiian watersheds, *in* 2nd Joint Federal Interagency Conference: Las Vegas, Nevada, 11 p.

Stone, J.O., 2000, Air pressure and cosmogenic isotope production: Journal of Geophysical Research–Solid Earth, v. 105, p. 23,753–23,759, doi:10.1029/2000JB900181.

Trenhaile, A.S., 2002, Modeling the development of marine terraces on tectonically mobile rock coasts: Marine Geology, v. 185, p. 341–361, doi:10.1016/S0025-3227(02)00187-1.

Tucker, G.E., 2009, Natural experiments in landscape evolution: Earth Surface Processes and Landforms, v. 34, p. 1450–1460, doi:10.1002/esp.1833.

Valla, P.G., van der Beek, P.A., and Carcaillet, J., 2010, Dating bedrock gorge incision in the French Western Alps (Ecrins-Pelvoux massif) using cosmogenic ^{10}Be: Terra Nova, v. 22, p. 18–25, doi:10.1111/j.1365-3121.2009.00911.x.

Vitousek, S., and Fletcher, C.H., 2008, Maximum annually recurring wave heights in Hawai'i: Pacific Science, v. 62, p. 541–553, doi:10.2984/1534-6188(2008)62[541:MARWHI]2.0.CO;2.

Watts, A.B., and Tenbrink, U.S., 1989, Crustal structure, flexure, and subsidence history of the Hawaiian Islands: Journal of Geophysical Research–Solid Earth and Planets, v. 94, p. 10,473–10,500, doi:10.1029/JB094iB08p10473.

Weissel, J.K., and Seidl, M.A., 1997, Influence of rock strength properties on escarpment retreat across passive continental margins: Geology, v. 25, p. 631–634, doi:10.1130/0091-7613(1997)025<0631:IORSPO>2.3.CO;2.

Weissel, J.K., and Seidl, M.A., 1998, Inland propagation of erosional escarpments and river profile evolution across the southeast Australian passive continental margin, *in* Tinker, K.J., and Wohl, E.E., eds., Rivers Over Rock: Fluvial Processes in Bedrock Channels: American Geophysical Union Geophysical Monograph 107, p. 189–206.

Wentworth, C.K., 1927, Estimates of marine and fluvial erosion in Hawaii: The Journal of Geology, v. 35, p. 117–133, doi:10.1086/623391.

Wentworth, C.K., 1928, Principles of stream erosion in Hawaii: The Journal of Geology, v. 36, p. 385–410, doi:10.1086/623529.

Whipple, K.X., 2004, Bedrock rivers and the geomorphology of active orogens: Annual Review of Earth and Planetary Sciences, v. 32, p. 151–185, doi:10.1146/annurev.earth.32.101802.120356.

Whipple, K.X., and Dunne, T., 1992, The influence of debris-flow rheology on fan morphology, Owens Valley, California: Geological Society of America Bulletin, v. 104, p. 887–900.

Whipple, K.X., and Tucker, G.E., 1999, Dynamics of the stream-power river incision model: Implications for height limits of mountain ranges, landscape response timescales, and research needs: Journal of Geophysical Research–Solid Earth, v. 104, p. 17,661–17,674, doi:10.1029/1999JB900120.

Whittaker, A.C., and Boulton, S.J., 2012, Tectonic and climatic controls on knickpoint retreat rates and landscape response times: Journal of Geophysical Research, v. 117, F02024, doi:10.1029/2011JF002157.

Willett, S.D., Slingerland, R., and Hovius, N., 2001, Uplift, shortening, and steady-state topography in active mountain belts: American Journal of Science, v. 301, p. 455–485.

Wobus, C.W., Crosby, B.T., and Whipple, K.X., 2006, Hanging valleys in fluvial systems: Controls on occurrence and implications for landscape evolution: Journal of Geophysical Research–Earth Surface, v. 111, F02017, doi:10.1029/2005JF000406.

Yanites, B.J., Tucker, G.E., and Anderson, R.S., 2009, Numerical and analytical models of cosmogenic radionuclide dynamics in landslide-dominated drainage basins: Journal of Geophysical Research–Earth Surface, v. 114, F01007, doi:10.1029/2008JF001088.

Ye, F., Barriot, J., and Carretier, S., 2013, Initiation and recession of the fluvial knickpoints of the Island of Tahiti (French Polynesia): Geomorphology, v. 186, p. 162–173, doi:10.1016/j.geomorph.2012.12.031.

Science Editor: A. Hope Jahren
Associate Editor: Anne Jefferson

Manuscript Received 22 May 2013
Revised Manuscript Received 19 November 2013
Manuscript Accepted 31 December 2013

Printed in the USA